Li *et al. Biochar* (2026) 8:75
https://doi.org/10.1007/s42773-026-00588-x

Biochar

ORIGINAL RESEARCH **Open Access**

Nitrogen conservation by hardwood biochar during food waste digestate composting: pyrolytic temperature dictates microbial mechanisms

Dongyi Li[1], Jun Zhou[2], Jialin Liang[3], Qiuxiang Xu[1], Jiayu Zhang[1], Wenhua Xue[1] and Jonathan W. C. Wong[1*]

Abstract

Food waste digestate (FWD) composting is hindered by severe nitrogen loss, primarily through ammonia (NH_3) and nitrous oxide (N_2O) emissions. While biochar amendment is known to mitigate this loss, the optimal pyrolysis temperature to maximize conservation remains unclear. This study decouples the distinct influence of pyrolysis temperature (300, 400, and 800 °C) of hardwood biochar on nitrogen conservation by linking biochar properties to microbial community dynamics. A critical trade-off is revealed: 300 °C biochar maximized NH_3 reduction (39.2% vs. control, $n = 2$, $p < 0.05$) but was coincided with the enrichment of *nirK/S*-harboring denitrifiers (e.g., *Luteimonas*), posing a potential challenge from increased N_2O emissions. Conversely, 800 °C biochar achieved the greatest N_2O reduction (47.5% vs. control, $n = 2$, $p < 0.05$), an outcome consistent with suppressed microbial denitrification. Critically, biochar produced at 400 °C achieved an optimal balance, likely through enhanced NH_3 adsorption and the fostering of a microbial community correlated with lower N_2O emissions, which ultimately led to a 46.3% reduction in total nitrogen loss (vs. control, $n = 2$, $p < 0.05$), the highest performance among all treatments. This work guides the selection of biochar pyrolysis temperature toward targeted nitrogen conservation and sustainable FWD valorization.

Highlights

- 400 °C biochar achieved the optimal balance, cutting total nitrogen loss by 46.3% for a higher-quality compost.
- A trade-off was observed: 300 °C biochar reduced ammonia, while 800 °C biochar was better at curbing the potent greenhouse gas nitrous oxide.
- The composting benefits came from biochar steering the microbial community, not just from its simple adsorption of gases.

Keywords Food waste digestate, Composting, Biochar, Nitrogen, Pyrolysis temperature

---

*Correspondence:
Jonathan W. C. Wong
jwcwong@associate.hkbu.edu.hk
Full list of author information is available at the end of the article

Graphical Abstract

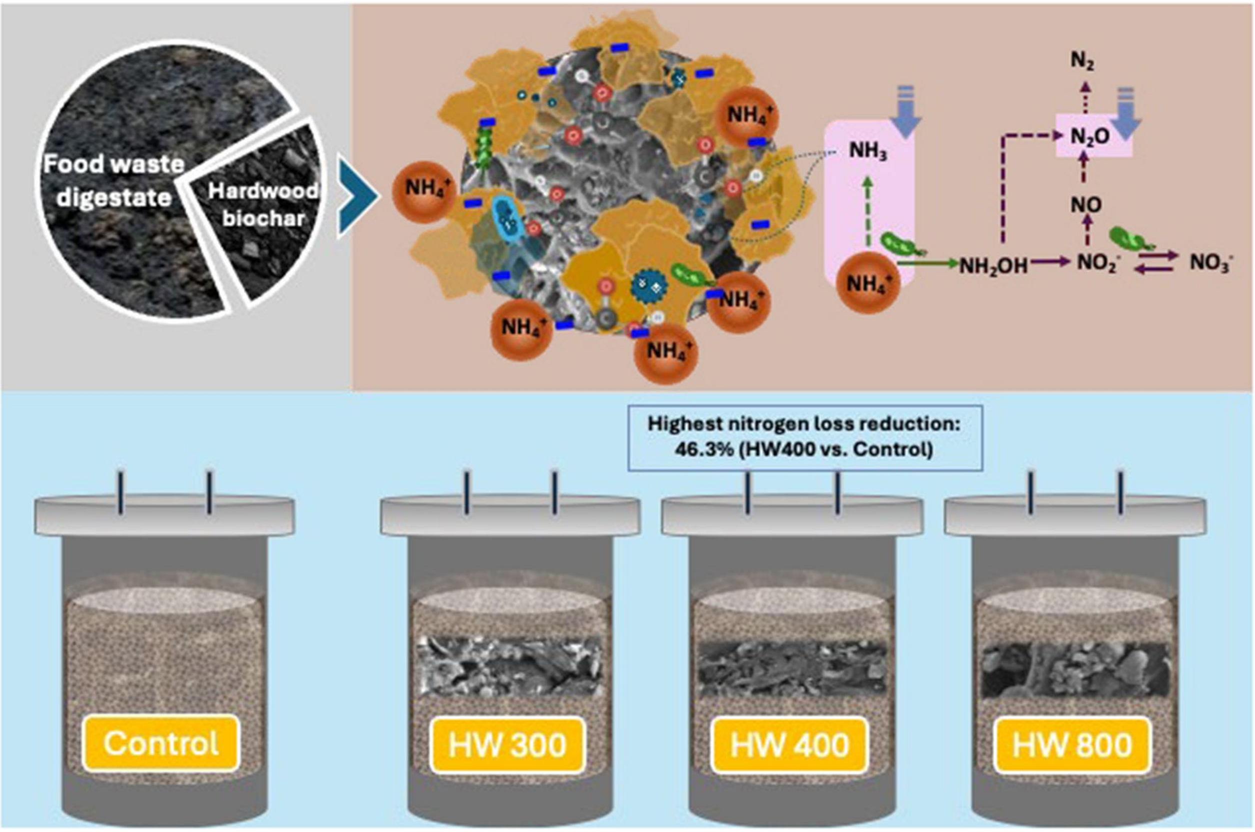

1 Introduction

The efficient recycling of food waste is a cornerstone of the circular bioeconomy (Dar et al. 2025). While anaerobic digestion (AD) recovers energy from food waste, it generates a nutrient-rich but challenging byproduct: food waste digestate (FWD) (Manu et al. 2021a). Composting of FWD is imperative for nutrient recycling, yet the process is fundamentally challenged by the material's intrinsic properties, i.e., high ammonium nitrogen content (NH_4^+-N > 8000 mg kg^{-1} dry matter (DM)), elevated moisture (~ 80%), and a low carbon-to-nitrogen (C/N) ratio (~ 6.9) (Li et al. 2023). These properties drive substantial nitrogen loss as high as 39% of initial nitrogen, predominantly through gaseous emissions of ammonia (NH_3) and nitrous oxide (N_2O) (Li et al. 2023; Song et al. 2021). NH_3 volatilization accounts for approximately 82% of total nitrogen loss, largely driven by the high NH_4^+-N concentration and alkaline pH (> 8.5) inherent in FWD, particularly during the thermophilic phase. Concurrently, N_2O emissions, comprising about 10% of total nitrogen loss and corresponding to an emission factor about 0.6 g N kg^{-1} dry matter (DM, of compost), are primarily attributed to incomplete nitrification and denitrification under fluctuating oxygen conditions (Liu et al. 2024). These losses degrade the agronomic value of the compost and contribute to atmospheric pollution and climate forcing, creating a critical barrier to sustainable FWD management.

Biochar, a carbonaceous material produced by pyrolysis, can mitigate nitrogen loss during composting through physicochemical adsorption and microbial regulation (Deng et al. 2023; Nguyen et al. 2022; Yin et al. 2021; Zhang et al. 2020). Its efficacy is strongly governed by pyrolysis temperature, which dictates key physicochemical attributes such as specific surface area, pore structure, surface functional groups, and aromatization (Li et al. 2015b). As pyrolysis temperature increases, the specific surface area and pore volume of biochar generally increase. Simultaneously, the H/C and O/C atomic ratios decrease as a result of the thermal decomposition and consequent loss of oxygen-containing functional groups, which is a direct indicator of advancing carbon aromatization. Biochar produced at lower temperature (e.g., 200–500 °C) retains oxygen-containing groups (−COOH, −OH), which enhance cation exchange capacity (CEC) and promote NH_3/NH_4^+ adsorption (Tomczyk et al. 2020; Yin et al. 2021). For instance, low-temperature willow-chip biochar (350 °C) cut NH_3 by 44% and enhanced compost nitrogen retention by 25% (Janczak et al. 2017). Li et al. (2015b) summarized that biochar produced at 300–500 °C significantly reduced NH_3 emissions during composting, whereas 700–900 °C biochar did not. In contrast, biochar produced at higher temperatures (e.g., 500–900 °C) develops extensive porosity and a more aromatic structure, which improves aeration and is associated with greater effectiveness in reducing N_2O emissions (Yin et al. 2021). Wang et al. (2021) found that 700–900 °C coconut-shell biochar lowered total nitrogen loss by 35.8%. This divergence in functionality underscores a fundamental trade-off: strategies optimized for curtailing one nitrogen-loss pathway may inadvertently exacerbate another.

Current understanding of this trade-off has largely focused on physicochemical factors, such as adsorption and abiotic interactions. However, a decisive and understudied dimension lies in temperature-dependent microbial regulation. Biochar is not an inert adsorbent but an ecological niche that shapes microbial community assembly and function. Lower-temperature biochar, abundant in oxygen-containing groups, can adsorb NH_4^+, NO_3^-, and NO_2^- through electrostatic interactions and hydrogen bonding, thereby forming nitrogen-enriched microsites (Hagemann et al. 2017). These microsites can stimulate nitrogen-cycling functional microbes carrying functional genes such as *amoA*, *nirK*/*nirS*, and *nifH*, including ammonia-oxidizing bacteria (AOB, e.g., Nitrosomonadaceae), nitrite-oxidizing bacteria (NOB, e.g., *Nitrospira*), and various denitrifiers nitrogen fixers (e.g., *Mycobacterium*, *Arthrobacter*, Rhodospirillaceae and Bradyrhizobiaceae) (Parasar & Agarwala 2025; Zhao et al. 2023). Conversely, higher-temperature biochar, with its larger specific surface area and elevated pH, may recruit N_2O-reducing microbes and upregulate related functional genes involved in nitrogen fixation, nitrification, and denitrification (Wang et al. 2023). The higher pH associated with high-temperature biochar, resulting from enhanced ash and alkali content (Liao et al. 2021), could potentially stimulate N_2O-reducing microbial activity, thereby contributing to reduced N_2O emissions, as suggested by studies in analogous systems (Balmuk et al. 2023). While these studies hint at a microbial mechanisms, a critical and systematic knowledge gap persists: it remains unclear how the specific functional groups within the nitrogen-cycling microbiome (e.g., AOB, NOB, *nirK/S*-type denitrifiers) are differentially regulated by biochar's temperature-dependent properties, and to what extent this microbiome-driven regulation, as opposed to mere physicochemical adsorptions, dictates the ultimate trade-offs between NH_3 and N_2O emissions. Critically, current understanding remains fragmented, and no systematic study has decoupled these microbial mechanisms from adsorption effects to link pyrolysis temperature directly to the steering of composting nitrogen cycling microbiomes.

Therefore, this study tests the central hypothesis that the pyrolysis temperature of biochar determines its nitrogen conservation efficacy in composting by specifically regulating key functional microbial groups. This study systematically examines the regulation of nitrogen dynamics in FWD composting by the hardwood biochar produced at 300 °C, 400 °C, 800 °C, focusing on the roles of functional group mediated adsorption and microbiome driven regulation. The resulting temperature selection framework aims to provide a practical foundation for developing scalable composting strategies that support the circular bioeconomy.

2 Materials and methods

2.1 Feedstock materials and experimental design

Dewatered FWD was collected from a centrifuge following anaerobic digestion in 4300 m^3 digester at Hong Kong Organic Resources Recovery Centre Phase 1 (35 °C, 23-day hydraulic retention time). Mature compost from the same site served as the inoculum, and locally procured sawdust was used as the bulking agent. Biochar was produced by slow pyrolysis of hardwood in a furnace under oxygen-limited conditions. The hardwood was heated at 10 K min^{-1} to 300, 400, or 800 °C, held for 15 min, and the resulting biochars were designated HW300, HW400, and HW800, respectively. Prior to composting, the biochar was ground to < 2 mm to ensure uniform mixing. Basic properties of composting materials are given in Table S1.

Laboratory scale composting experiments were conducted in 20 L reactors, each consisting of an insulated tank with a sealed cover. An automatic temperature regulation system was implemented to minimize conductive heat loss. The core temperature (T_core) of the compost and the temperature of the insulated outer tank wall (T_wall) were continuously monitored using PT100 sensors. The control algorithm was based on the real-time temperature difference ($\Delta T = T\_core—T\_wall$) between these two points. When ΔT exceeded a set threshold of 3 °C, indicating excessive heat loss from the core, heating cables embedded in the insulation layer were activated to reduce the thermal gradient and conserve metabolic heat. Aeration was provided at a base rate of 0.25 L min^{-1} kg^{-1} DM through a bottom inlet, controlled by a flow meter, while supplementary ventilation was provided when the temperature of the composting mixture was above 65 °C during the thermophilic phase to manage heat dissipation. Temperature data were continuously recorded using automated software. A schematic of the reactor system is provided in Fig. S1 (Song et al. 2021).

Four treatment groups were established, including one Control treatment (R1) and three with the 10% addition of biochar (dry weight basis) produced at 3 different pyrolytic temperatures (R2: 300 °C, R3: 400 °C, and R4: 800 °C). This dosage was selected as it has been shown effective for improving nitrogen conservation and composting processes in prior studies (Manu et al. 2021a, 2021b; Awasthi et al. 2020). To produce a C/N ratio of ~20 and a moisture content of 55%, a digestate-sawdust-compost ratio of 1:1.6:0.5 (dry weight basis) was used based on the raw material's properties. All treatments were conducted in duplicate over a 42-day composting period. Throughout the experiment, the compost was turned manually at every sampling time point.

2.2 Sampling and analysis

Approximately 200 g of compost sample was collected from each reactor after thorough mixing on days 0, 3, 7, 14, 21, 28, and 42. Each sample was split into two portions: one stored at 4 °C for immediate physicochemical analyses, and the other stored at −80 °C for subsequent biological analyses.

2.2.1 Biochar characterization

The functional groups in hardwood biochar samples were assessed via Fourier Transform Infrared Spectroscopy (FT-IR, Two FT-IR Spectrometer, PerkinElmer) within the wave number range of 4000 cm^{-1} to 500 cm^{-1}. Morphological features were examined using a scanning electron microscope (SEM, Zeiss, Germany). The Brunauer–Emmett–Teller (BET) surface area and pore size distribution were determined with a Surface Area & Porosimetry System (Micromeritics ASAP 2460, Japan) (He et al. 2019). Cation Exchange Capacity (CEC) was determined via the ammonium acetate (NH_4OAc) saturation method at pH 7.0. The pH at the point of zero charge (pH_pzc) was determined by measuring the zeta potential of samples dispersed in deionized water over a pH range of 3–11 (adjusted with HCl/NaOH) using a Zetasizer (Malvern, England). The pH_pzc was taken as the point where the zeta potential–pH curve crossed zero (Fig. S2).

2.2.2 Physicochemical parameters

Moisture content (MC), pH, electrical conductivity (EC), extractable ammonium (NH_4^+-N), nitrate (NO_3^--N), nitrite (NO_2^--N), seed germination index (SGI), total nitrogen (TN), and total carbon (TC) were analyzed using the following methodologies. Approximately 30 g compost was oven-dried at 105 °C for 24 h to determine MC. 20 g fresh samples were extracted with deionized water at a solid-to-liquid ratio of 1:5 (dry weight equivalent, w/v). The volume of deionized water added was adjusted based on the moisture content of the fresh sample to achieve this final ratio. The extractant, obtained after shaking for 1 h, was analyzed according to the standard method for compost analysis outlined in the Test Methods for the Examination of Composting and Compost (TMECC 2015). The resulting suspensions were used to measure pH and EC using a pH meter (Orion Star™ A111 Benchtop pH Meter, Thermo Scientific™) and an EC meter (Orion Star™ A112 Benchtop Conductivity Meter, Thermo Scientific™), respectively. Subsequently, the suspensions were centrifuged at 13,000 rpm for 10 min and filtered through 0.45 μm membrane filters for the determination of extractable NH_4^+-N, NO_3^--N, NO_2^--N, and SGI. NH_4^+-N was determined using the indophenol-blue method, while NO_3^-/NO_2^- was determined by flowing injection analysis (QuikChem 8500 series 2, Lachat instrument). TN and TC were determined using CHNS (Elementar vario MACRO, Germany). For the SGI test, 5 mL of each testing solution was pipetted onto a sterilized petri-dish with a Whatman No. 1 filter paper. Blank sample was made using distilled water instead of the mixture extract. Ten cress seeds (*Lepidium sativum*) were placed in each petri dish and incubated in darkness for 48 h at 25 °C. The SGI was calculated by counting the number of germinated seeds and measuring the length of root radical (Eq. 1) (Manu et al. 2021b; Zucconi 1981).

$$SGI(\%) = (seed\ germination\ rate\ of\ compost\ sample \times root\ length\ of\ compost\ sample) / (seed\ germination\ rate\ of\ blank\ sample \times root\ length\ of\ blank) \times 100\% \tag{1}$$

where the blank denotes the deionized water control.

2.2.3 Gaseous emissions measurements

Gaseous emissions, including NH_3, N_2O, and CO_2, were measured daily during the composting process using gas analyzers (Guangzhou Kun Lian Technology Co., Ltd). Gas emitted from the composters was directed through a silica-gel drying tube to remove moisture, collected in gas bags, and subsequently analyzed using gas analyzers via the syringe sampling method. The concentration of

CO_2 was monitored as an indicator of overall microbial respiratory activity, and its emission profile is provided in the supplementary file (Fig. S3). Concentrations of each gaseous emission were converted to emission rates using the following formula (Eq. 2) (Li et al. 2023):

$$N = (C \times A \times M) / (m \times V) \tag{2}$$

where N represents the gas emission rate; C denotes the concentration of the individual gas in ppm; A is the air flow rate in L kg^{-1} min^{-1}; M signifies the molar mass of the gas in g mol^{-1}; m stands for the dry matter of the initial composting mass in kg; and V indicates the molar volume of the gas in L mol^{-1}. The gaseous emission losses were calculated based on the cumulative emission data with respect to the initial nitrogen mass.

The nitrogen loss within the system was calculated using the following formula (Eq. 3):

$$\begin{aligned} &Nitrogen\ loss\ (\%) = (\%) \\ &= [(TN\ initial \times DM\ initial) - (TN\ final \times DM\ final)] \\ &\ / (TN\ initial \times DM\ initial) \times 100\% \end{aligned} \tag{3}$$

where *Nitrogen loss* (%) is the percentage of total nitrogen lost; *TN* denotes the total nitrogen content; *DM* represents the dry matter mass; subscripts *initial* and *final* refer to the beginning and end of the composting period, respectively.

The proportions of individual gaseous nitrogen losses relative to the initial total nitrogen were calculated separately for NH_3 and N_2O using Eqs. 4 and 5:

$$NH_3\ loss\ (\%) = \sum (NH_3\ emission) / (TN\ initial \times DM\ initial) \times 100\% \tag{4}$$

$$N_2O\ loss\ (\%) = \sum (N_2O\ emission) / (TN\ initial \times DM\ initial) \times 100\% \tag{5}$$

where $\Sigma(emission)$ represents the cumulative mass of the respective gas emitted over the composting period.

System boundaries were defined as follows: Input was the total initial nitrogen, comprising the nitrogen content of all raw materials (FWD, sawdust, mature compost, etc.) and any nitrogen added via biochar. Output encompassed all nitrogen leaving the system, including: retained nitrogen (measured in the final product); measured gaseous nitrogen (cumulative emissions of NH_3 and N_2O); unmeasured gaseous nitrogen (e.g., N_2 and NO_x emissions, considered minor); and sampling-associated nitrogen loss (a quantified margin of error in the mass balance).

2.3 Metagenomic analysis

The representative samples were collected at selected stages of composting on days, 0, 7, 42, representing the initial status, thermophilic phase, and maturation phase, respectively. For each treatment at each time point except day 0, the sample from the two replicate reactors was composited and homogenized to form a single, representative sample prior to DNA extraction, therefore total metagenomic sample number was 9 (Ajuna et al. 2020). The total genomic DNA of each compost sample was extracted from a 500 mg sample using DNeasy Power Soil Pro Kit (QIAGEN, Hilden, Germany). The purity and concentration of DNA were determined by microspectrophotometer (NanoDrop ND-2000, Thermo Fisher Scientific, USA). The extracted DNA samples were stored at −20 °C until microbial analysis submission. Sequencing was conducted by Majorbio Bio-Pharm Technology Co., Ltd. (Shanghai, China) on an Illumina NovaSeq 6000 platform using the NovaSeq 6000 S4 Reagent Kit (300 cycles), with an average insert size of 500 bp, following the manufacturer's protocol (www.illumina.com). The run generated 2×150 bp paired-end reads, with an average sequencing depth of ~6 Gb per sample. On average, 46.2 million raw paired-end reads (150 bp) were generated per sample, yielding approximately 6.98 Gb of raw data. Stringent quality control was conducted using Fastp (https://github.com/OpenGene/fastp, v0.20.0) with a Phred score threshold of ≥ 20. After filtering, >95% of reads and >94% of bases were retained, ensuring high-quality data for all downstream analyses. The obtained raw sequence data were then utilized for further analysis. Metagenomic assembly was performed using Megahit (https://github.com/voutcn/megahit, v1.1.2), and fragments smaller than 500 bp were filtered out (Li et al. 2015a). Open reading frames in the assembled contig sequences were predicted using the Prodigal software (https://github.com/hyattpd/Prodigal, v2.6.3) (Hyatt et al. 2010). For the generation of a non-redundant gene set, CD-HIT (http://www.bioinformatics.org/cd-hit/, v4.6.1) eliminated redundancy from the predicted gene sequences (Fu et al. 2012), SOAPaligner (http://soap.genomics.org.cn/, v2.21) facilitated the comparison of sequence data with the constructed non-redundant gene set (with a similarity 0.95), enabling the calculation of individual gene abundances in different samples (Li et al. 2009). Phylum- and genus-level abundances were derived through protein annotation. Taxonomic classification was performed by aligning the non-redundant gene set against the NCBI NR database (release 20,230,830) using DIAMOND (http://www.diamondsearch.org/index.php, v2.0.13) in BLASTP mode with an e-value cutoff of $1e^{-5}$. The resulting alignments were assigned taxonomy using the corresponding taxonomic information of the NR database. The abundance of each taxon at each level (from domain to species) was then calculated by summing the abundances of its associated genes, thereby constructing the abundance profiles reported in the study

Table 1 Basic properties of hardwood biochar

Property	HW300	HW400	HW800
pH (solid: water = 1:5)	8.57	9.20	10.20
Surface area (BET, m^2 g^{-1})	9.17	15.99	19.87
Total pore volume (SPA, cm^3 g^{-1})	0.031	0.076	0.072
Average pore diameter (AAPD, nm)	10.42	12.07	11.94
Cation exchange capacity (CEC, cmol kg^{-1})	16.8	15.8	13.7
Point of zero charge (pH$_p$zc)	3.37	4.00	< 3
C (%)	60.36	60.11	66.09
H (%)	3.65	3.54	2.00
N (%)	2.04	1.86	1.52
O (%)	22.83	22.84	13.31

BET Brunauer–Emmett–Teller, *SPA* Single point adsorption, *AAPD* Adsorption average pore diameter (4 V/A by BET).

CEC was determined by the NH_4OAc saturation method (pH 7.0).

The pH$_p$zc was determined by measuring the zeta potential as a function of pH in deionized water using a Zetasizer.

(Buchfink et al. 2015; Xie et al. 2011). Functional annotation of the gene set was performed using DIAMOND (v2.0.13) for a BLASTP search (e-value threshold: 1e^{-5}) against the Kyoto Encyclopedia of Genes and Genomes (KEGG; http://www.genome.jp/kegg/, release 202,209) database to predict metabolic pathways. Metagenomic sequence reads are available in the NCBI SRA database under the accession PRJNA1377318.

2.4 Statistical analysis

Data on compost properties and gas production were analyzed using analysis of variance (ANOVA). When ANOVA indicated significant effects ($p < 0.05$), Duncan's multiple range test was applied for post-hoc comparison of means.

3 Results and discussion

3.1 Influence of pyrolytic temperature on biochar properties

The pyrolytic temperature critically determines the physicochemical properties of the hardwood biochar (Table 1) (Kalina et al. 2022). As expected, both pH and BET surface area increased with rising pyrolytic temperature (Sahoo et al. 2021). However, the evolution of porosity followed a non-monotonic trend: while specific surface area rose steadily, total pore volume and average pore diameter peaked at 400 °C, likely due to optimal devolatilization of biomass. At 800 °C, the decrease in these parameters suggests the possible collapse of larger pores formed at lower temperatures, even as microporosity continued to develop. These structural changes are visually evident in SEM images, which show a progression from a dense morphology with sharp edges at 300 °C (Fig. 1a) to more porous but partially fused structures at higher temperatures (Fig. 1b, c) (Adesemuyi et al. 2020; Li et al. 2015b). The H/C and O/C atomic ratios of hardwood biochar decreased with increasing pyrolysis temperature.

Figure 1d illustrates the variation in FTIR spectra of biochar with changing pyrolytic temperatures. As the temperature increased, distinct bonds from the wood, primarily associated with aromatic C–H out-of-plane bending (885–750 cm^{-1}), symmetric C–O stretching for cellulose, hemicelluloses and lignin (1026 cm^{-1}), and C=C aromatic ring stretching (1609–1440 cm^{-1}) were retained (Liu et al. 2015). The O–H bending of phenols was observed at 1375 cm^{-1} for HW300 and HW400 but absent in HW800 (Cantrell et al. 2012). The peak at 1609 cm^{-1} can be attributed to aromatic C=C stretching and C=O stretching modes of conjugated ketones and quinones, more pronounced in HW300 and HW400. Additionally, the peaks at 2920 and 2848 cm^{-1} were attributed to $-CH_3$ and $-CH-/-CH_2$, respectively, but were absent in HW800. The broad peak at 3280 cm^{-1} represents the O–H stretching vibrations of hydrogen-bonded hydroxyl groups, indicating the presence of carboxylic acid or water adsorption, which is observed only in biochar from lower pyrolytic temperatures (HW300 & HW400) (Cole et al. 2019; Tan et al. 2020). In comparison to HW800, the HW300 and HW400 spectra show more peaks overall, suggesting that there are more functional groups on the surface of the biochar and that these groups persist at lower pyrolytic temperatures. This observation aligns with the decrease in H/C and O/C atomic ratios, which reflects a higher degree of aromatic condensation at elevated temperatures and consequently fewer functional groups (Adesemuyi et al. 2020; Tomczyk et al. 2020).

3.2 Variation in temperature, pH, and EC during composting

All treatments reached temperatures > 55 °C by day 2, with the duration of this phase lasting 9, 8, 8, and 10 days for the Control, HW300, HW400, and HW800, respectively, indicating vigorous aerobic microbial activity (Fig. 2a) (Wang et al. 2025). Temperatures dropped briefly after turning but recovered rapidly. Statistical analysis revealed no significant differences in temperature profiles among treatments during the first 10 days ($p \geq 0.05$), consistent with their identical initial composition. Given the identical initial composition, this statistical uniformity suggests that the FWD substrate composition was the dominant factor governing the initial thermal regime. Following a week, all treatments' temperatures started to drop gradually, entering the cooling phase, indicating the commencement of the maturation (Hoseini et al. 2025).

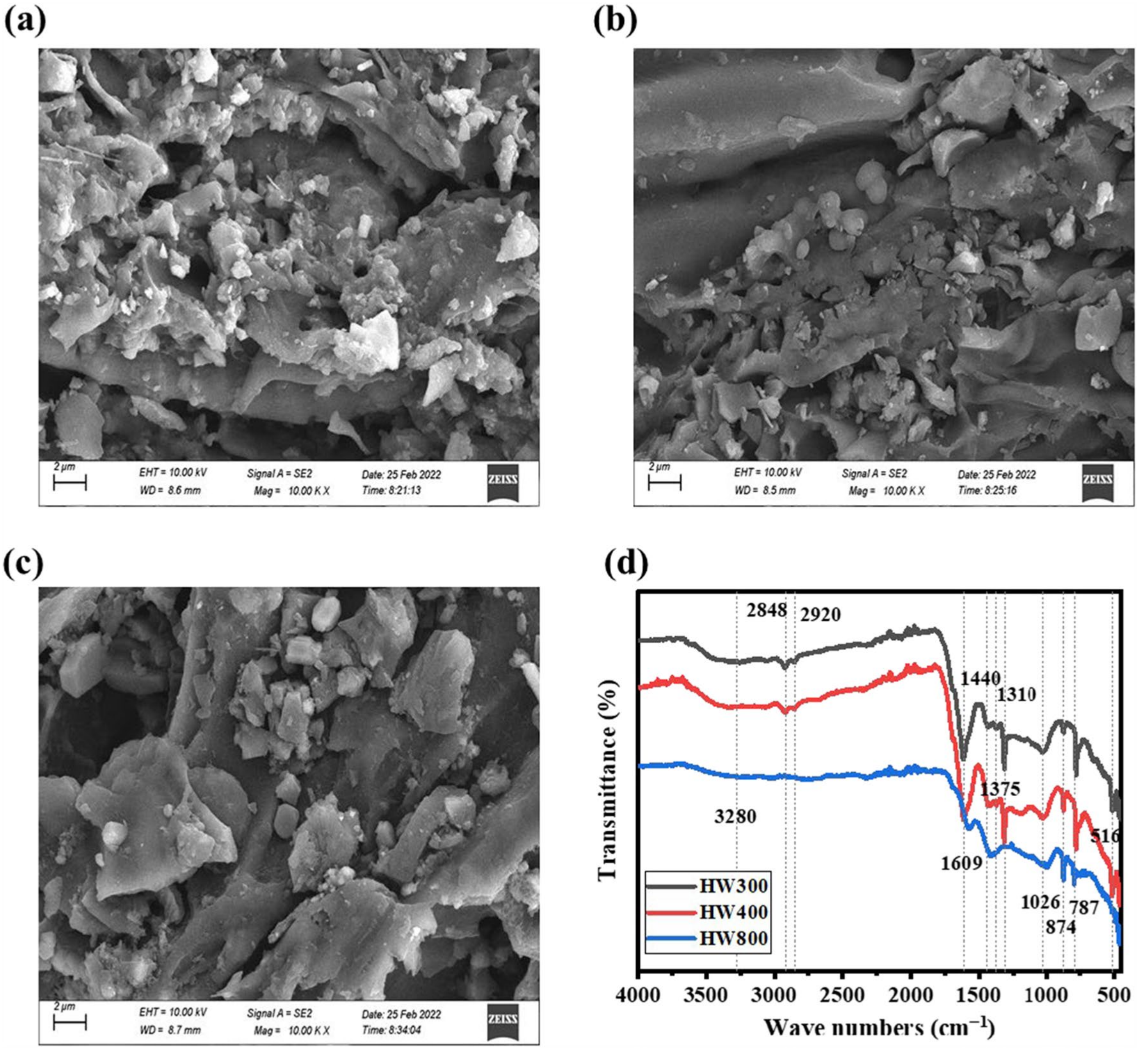

Fig. 1 Scanning electron micrographs of hardwood biochar prepared at 300 °C (**a**), 400 °C (**b**), and 800 °C (**c**); and the Fourier transform infrared spectroscopy analysis of the hardwood biochar pyrolyzed at different temperatures (**d**)

pH initially decreased in all treatments (Fig. 2b), which may be attributable to organic acid release during early decomposition, followed by an increase peaking around day 14—a pattern consistent with other composting studies (Ma et al. 2024; Tian et al. 2023). As composting progressed, pH values decreased to 6.12, 6.55, 6.81, and 7.23 in the Control, HW300, HW400, and HW800 treatments, respectively, indicating mature compost formation (Manu et al. 2022). This decrease was attributed to nitrification, which produces protons and acidifies the compost, along with the accumulation of small-molecule organic acids (Tian et al. 2023). Biochar additions provided a buffer against the decrease in pH, resulting in a higher pH for the mature compost (Manu et al. 2021b).

EC fluctuated in the early stage from an initial ~ 7 mS cm^{-1} (Fig. 2c). The initial decrease in EC might be associated with the concurrent decline in NH_4^+-N concentration (Fig. 3a) and NH_3 volatilization (Fig. 3d, e), although contributions from other ions cannot be ruled out. Later increases likely resulted from salt concentration during organic matter mineralization. Overall, the lower final EC values in biochar treatments suggest that soluble ions were either adsorbed onto the biochar or diluted by its addition, or that both processes occurred together (Huang et al. 2024). Among all treatments, HW400 had the lowest EC, likely attributed to the integrated factors of the diverse functional groups on its surface and a relatively higher surface area, resulting in a stronger adsorption capacity (Olivera-Begue et al. 2025).

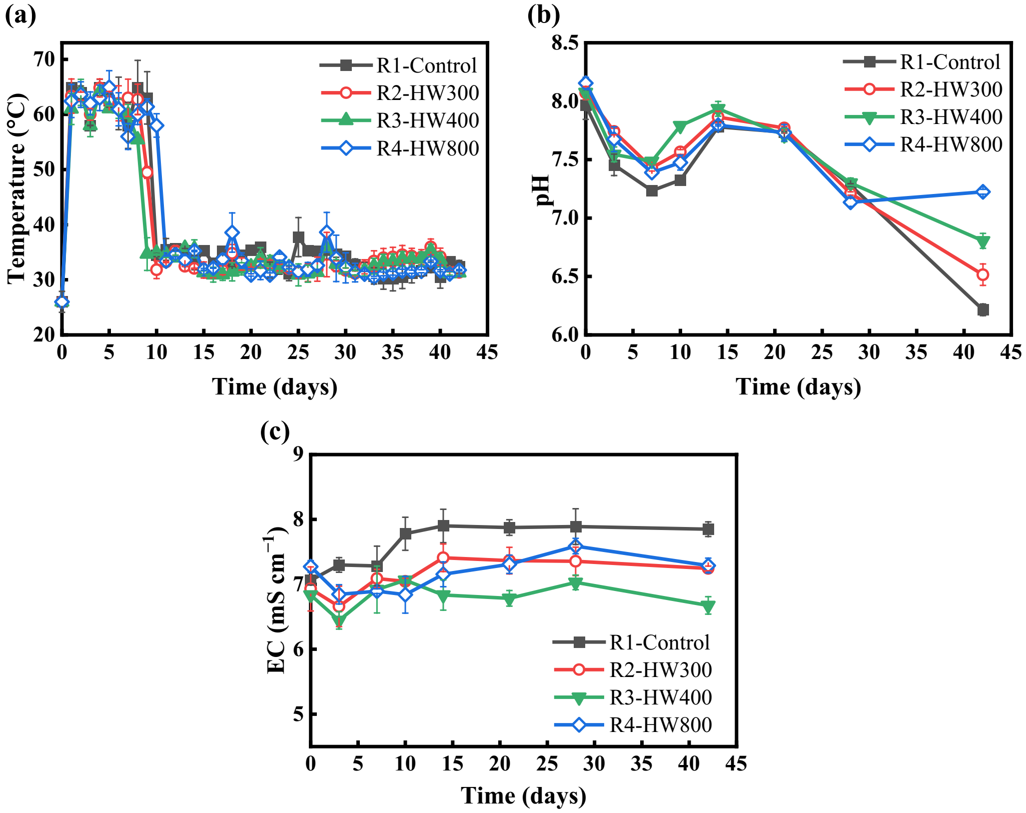

Fig. 2 Dynamic changes of the temperature (**a**), pH (**b**), and EC (**c**) during the composting of food waste digestate amended with hardwood biochar prepared at 300 °C (R2), 400 °C (R3) and 800 °C (R4) as compared to the Control without biochar amendment (R1)

3.3 Nitrogen transformation during composting

The initial NH_4^+-N contents were approximately 2000 mg kg^{-1} DM and decreased throughout composting (Fig. 3a). Its dynamics exhibited a two-phase pattern. The initial rapid decline within the first 10 days might be attributed to NH_3 volatilization under thermophilic conditions. Consistently, the HW800 treatment, which showed the highest NH_3 emission (Fig. 3d, e), reached the lowest NH_4^+-N level in this phase. In the subsequent phase, the NH_4^+-N level in HW800 decreased in a slower rate and maintained a higher concentration than other treatments gradually. This pattern was likely due to the higher specific surface area and lower pH_pzc of biochar produced at high temperature, which would promote NH_4^+ retention through adsorption (He et al. 2021, 2019; Nguyen et al. 2023). Meanwhile, a distinct and sustained decline of NH_4^+-N level became prominent in treatments amended with biochars produced at lower temperature (HW300 & HW400). This decline correlated with a significant rise in NO_2^--N and NO_3^--N concentrations (Fig. 3b, c), indicating a shift toward active microbial nitrification as the dominant NH_4^+ removal process (Fang et al. 2023). Consequently, HW300 and HW400 treatments reached the acceptable NH_4^+-N level (< 500 mg kg^{-1} DM) by days 30 and 25, respectively, notably sooner than HW800 (day 38) and the Control (> 42 days). This pattern suggests that while HW800 biochar may retain more NH_4^+-N via adsorption, biochars produced at lower temperature (HW300 & HW400) might foster more effectively microbial communities that would drive efficient nitrification, thereby accelerating the reduction of NH_4^+-N toxicity during the curing phase.

Nitrification, which plays a crucial role in nitrogen conservation during composting with NO_2^- acting as an intermediate product during nitrification catalyzed by AOB, typically exhibits an initial increase followed by a subsequent decrease (Cáceres et al. 2018). Following the decrease in NH_4^+-N, nitrification occurred from day 14 in all the treatments and the concentration of NO_2^--N peaked on day 21 for HW300, while all other treatments peaked on day 28. Corresponding with the fastest decrease in NH_4^+-N, HW300 achieved the highest peak for NO_2^--N of 215.8 mg kg^{-1} DM, followed by HW400 (170.5 mg kg^{-1} DM), HW800 (150.1 mg kg^{-1} DM), and the Control (110.8 mg kg^{-1} DM) (Fig. 3b). The specific

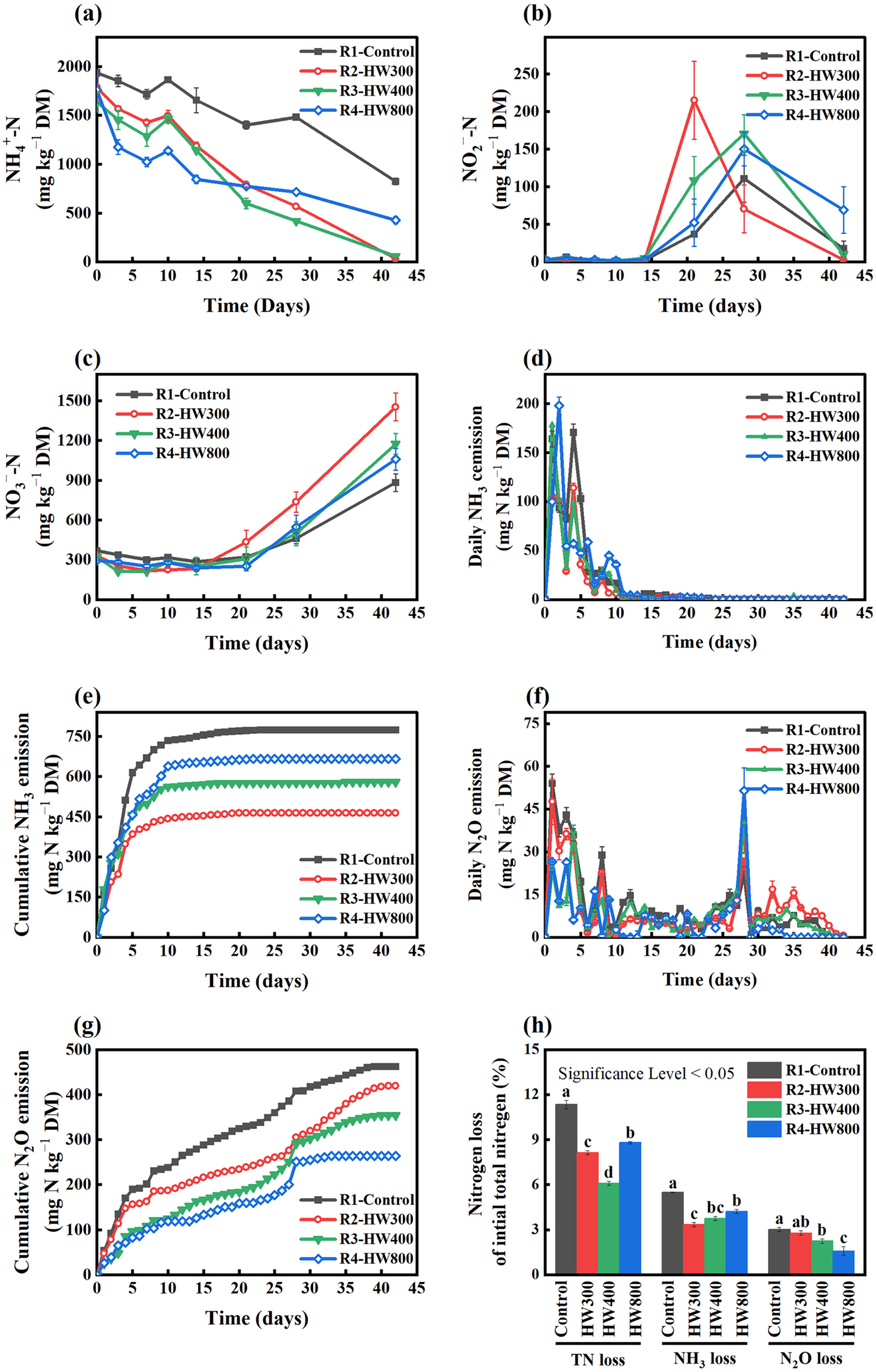

Fig. 3 Transformation of nitrogen species including NH_4^+-N (**a**), NO_2^--N (**b**), NO_3^--N (**c**), NH_3 emissions (**d**), cumulative NH_3 emissions (**e**), N_2O emissions (**f**), cumulative N_2O emissions (**g**), and nitrogen balance (**h**) during the composting of food waste digestate amended with hardwood biochar prepared at 300 °C (R2), 400 °C (R3) and 800 °C (R4) as compared to the Control without biochar amendment (R1)

pyrolytic temperature of biochar at 300 °C clearly demonstrated its effectiveness in the conversion of NH_4^+-N to NO_2^--N. The changes in NO_3^--N during the composting process as shown in Fig. 3c. NO_3^--N of HW300 commenced to increase on day 14 and then reached the highest level of 1454.55 mg kg^{-1} DM at the end of the composting process, while all other treatments had only commenced on day 21 and reached the peak NO_3^--N concentrations of 1174.9, 1058.3, and 872.4 mg kg^{-1} DM in the HW400, HW800, and Control treatments, respectively (Fig. 3c). Wang et al. (2023) also showed that biochar facilitates NH_4^+-N to NO_3^--N conversion. However, the present study confirms clearly biochar prepared at a low pyrolytic temperature of 300 °C performs better than that prepared at a higher temperature of 800 °C in the perspective of nitrification process during composting. Interestingly, Agyarko-Mintah et al. (2017a, b) found that the Control treatment exhibited the highest NO_3^--N concentration compared to biochar amendments, suggesting variability in biochar's impact on nitrification. This inconsistency may be attributed to biochar's potential to reduce nitrification by adsorbing NH_3/NH_4^+ within its pore structure, inhibiting nitrifiers sensitive to high NH_3/NH_4^+ levels and alkaline conditions.

NH_3 emission during composting is highlighted as a significant issue that can compromise the quality of the final compost product (Zhang et al. 2016). The release of NH_3 was particularly concentrated during the first week thermophilic phase with up to 80% of total amount of NH_3 evolved during the composting (Fig. 3d) (Manu et al. 2022), which could be attributed to the alkalinity and high temperature of the raw materials favourable for promoting NH_3 emissions. The addition of hardwood biochar could help mitigate NH_3 emissions during the composting process by absorbing NH_3/NH_4^+, resulting in a lower cumulative NH_3 emission, potentially involving mechanisms such as surface complexation, electrostatic interaction, and ion exchange (Agyarko-Mintah et al. 2017b; Ambaye et al. 2020; Hu et al. 2020). The higher CEC and enhanced nitrification process in the HW300 treatment likely offset its lower surface area, leading to the lowest cumulative NH_3 emissions (464.1 mg N kg^{-1} DM). Emissions were higher for HW400 (579.4 mg N kg^{-1} DM) and HW800 (666.5 mg N kg^{-1} DM) (Fig. 3e). The HW300 treatment exhibited the most substantial mitigation in NH_3 emission, followed by HW400 and HW800, which aligns with previous findings (Li et al. 2015b). Notably, HW300 and HW400 demonstrated more effective reduction in NH_4^+-N. This observation may be attributed to the diverse functional properties of the biochar surface produced under lower temperatures, resulting in enhanced NH_4^+/NH_3 adsorption (Li et al. 2015b; Wang et al. 2023). However, further experiments, such as nutrient release experiments from composted hardwood biochar or adsorption/desorption experiments for the hardwood biochar, are needed to confirm this assumption. Alternatively, the reduction of NH_3 emission in the lower pyrolytic temperature biochar treatment was amplified by the effective nitrification, thus leading to the overall reduction of NH_3 emission. Overall, the findings suggest that incorporating hardwood biochar into the composting process can effectively reduce NH_3 emissions, with the HW300 treatment exhibiting the most significant mitigation effect, followed by HW400 and HW800.

N_2O, a potent greenhouse gas, constitutes another pathway of nitrogen loss during composting (Tang et al. 2020; Wu et al. 2021). Its emissions exhibited a biphasic pattern (Fig. 3f). The initial emission phase (days 0–10) is attributed to denitrification, a process where microbes consume NO_3^- as an alternative electron acceptor, explaining its observed decline in the first week (Angnes et al. 2013; Gao et al. 2021). Additionally, another peak in N_2O emissions occurred in all treatments on day 28, which is likely due to the combined processes of nitrification and denitrification by nitrifiers and denitrifiers (Fu et al. 2022; Shangguan et al. 2022). The peak daily N_2O emission flux on day 28 increased markedly with biochar pyrolysis temperature, with mean values of 22.2, 28.6, 40.2, and 51.4 mg N kg^{-1} DM d^{-1} for the Control, HW300, HW400, and HW800 treatments, respectively ($p \geq 0.05$). Notably, the flux for HW800 was significantly higher than that for the Control ($p < 0.05$), indicating that higher-temperature biochar may create conditions that intensify the nitrification–denitrification activity responsible for this emission pulse. In contrast to the peak fluxes, the cumulative N_2O emissions over the entire composting period were substantially reduced by biochar amendment (Fig. 3g), measuring 462.2, 419.6, 353.7, and 263.9 mg N kg^{-1} DM for Control, HW300, HW400, and HW800, respectively. This indicates a strong overall mitigation effect, which was more pronounced for higher temperature biochars (HW400/HW800). This reduction is likely due to the porous structure of biochar, which improves the oxygen diffusion leading to a reduction of anaerobic zones. This physical alteration likely suppresses incomplete denitrification (N_2O production) and may promote more complete denitrification to N_2. This inference is supported by the higher ratio of *nosZ* to *nor* observed in the nitrogen pathway (Fig. 6a), which was consistent with lower cumulative N_2O emissions (Fukumoto et al. 2006). Additionally, the higher residual NH_4^+-N pool in the Control treatment may represent a prolonged substrate source that could sustain nitrification-mediated N_2O production, warranting attention in future studies.

Figure 3h illustrates the nitrogen mass balance during the FWD composting process. The ratios of total nitrogen loss based on the initial total nitrogen content were 11.34% (Control), 8.13% (HW300), 6.09% (HW400), and 8.8% (HW800). Consequently, the addition of HW400 biochar resulted in a 46.3% reduction in nitrogen loss as compared to the Control, showcasing its efficacy ($p < 0.05$). HW300 and HW800 also showed significant reductions of 28.3% and 22.4% ($p < 0.05$), respectively, in nitrogen loss compared to the Control, attributed to the reduction of NH_3 and N_2O emission facilitated by the biochar. NH_3 loss as a percentage of initial nitrogen was calculated to be 5.49%, 3.34%, 3.75%, and 4.22% for the Control, HW300, HW400, and HW800 treatments, respectively. This indicates that hardwood biochar has the potential to reduce NH_3 emissions by 23.1% to 39.2%, with HW300 showing the highest reduction (vs. control, $n = 2$, $p < 0.05$). On the other hand, 3.01%, 2.78%, 2.24%, and 1.58% of initial nitrogen was lost in the form of N_2O in the Control, HW300, HW400, and HW800 treatments, respectively. As a result, HW800 exhibited the most effective mitigation of N_2O emission, demonstrating a 47.5% reduction compared to the Control ($n = 2$, $p < 0.05$). The findings suggest that lower temperature pyrolytic biochar has greater potential to reduce NH_3 emissions, likely due to its diverse functional groups on the surface. On the other hand, higher pyrolytic temperature biochar excels in mitigating N_2O, attributed to its higher surface area. Overall, HW400 proved to be the most effective in reducing total nitrogen loss, indicating its potential as an amendment in FWD composting.

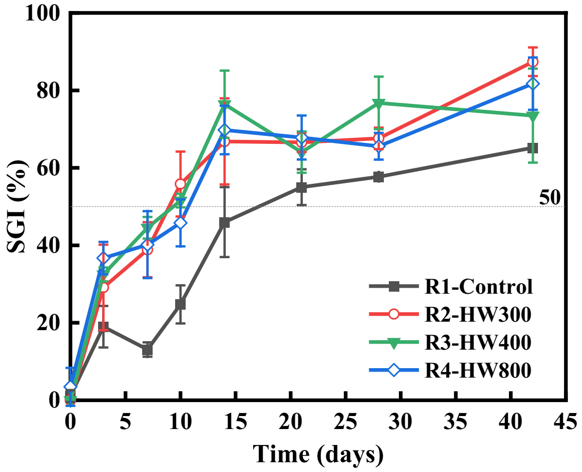

Fig. 4 Evolution of the seed germination index (SGI) during the composting of food waste digestate amended with hardwood biochar prepared at 300 °C (R2), 400 °C (R3), and 800 °C (R4) as compared to the Control without biochar amendment (R1)

3.4 Assessment of compost maturity

The SGI serves as a reliable indicator of compost maturity and phytotoxicity (Fu et al. 2025). Initially low SGI values likely stemmed from the release of toxic substances during active decomposition, such as NH_4^+-N and volatile organic acids (Wang et al. 2025). Biochar amendments accelerated maturation: treatments HW300 and HW400 reached the maturity threshold (SGI > 50%) by day 8, and HW800 by day 10, compared to 21 days for the Control (Fig. 4) (Li et al. 2023). Final SGI values were significantly higher in biochar treatments (73.5–87.4%) than in the Control (65.2%). Compost maturity was further corroborated by two additional biological indicators. First, nitrification was completed in all treatments, with final NO_3^-/NH_4^+ ratios exceeding the recognized threshold of 1 (ranging from 1.07 to 43.00) (Fig. 3a, c). This signifies the establishment of a stable nitrifying community and the disappearance of conditions inhibitory to these bacteria, a key marker of biochemical stability (Azim et al. 2018). Second, microbial metabolic activity was stabilized as indicated by the decline of CO_2 evolution rate for all treatments at a level below 6.68 g CO_2 kg^{-1} DM day^{-1} (equivalent to ≤ 2 g C kg^{-1} VS day^{-1}) prior to day 42 (Supplementary Fig. S2). This indicated the depletion of readily decomposable organic matter. Therefore, the integrated assessment based on phytotoxicity removal (SGI), nitrification dynamics, and respiration activity confirms the production of a mature and stable compost across all biochar-amended treatments.

3.5 Microbial community dynamics and their association with nitrogen metabolism

3.5.1 Characteristics of bacterial community during composting

Day 0, 7, and 42 samples have been chosen to represent the microbial community at the initial, thermophilic, and mature stages during composting. The microbial community structure at phylum level is depicted in Fig. 5a. Proteobacteria (30.7%), Firmicutes (16.1%), Deinococcus-Thermus (11.8%), Bacteroidota (11.5%), Actinobacteria (10.3%), Euryarchaeota (6.4%), and Chloroflexi (2.5%) collectively accounted for 89.3% of the average relative abundance across all samples during the entire composting process.

The taxonomic distribution of dominant phylum at the initiation of composting (day 0) revealed the presence of Firmicutes (39.48%), Proteobacteria (7.2%), Bacteroidota (17.07%), Actinobacteria (3.4%), Euryarchaeota

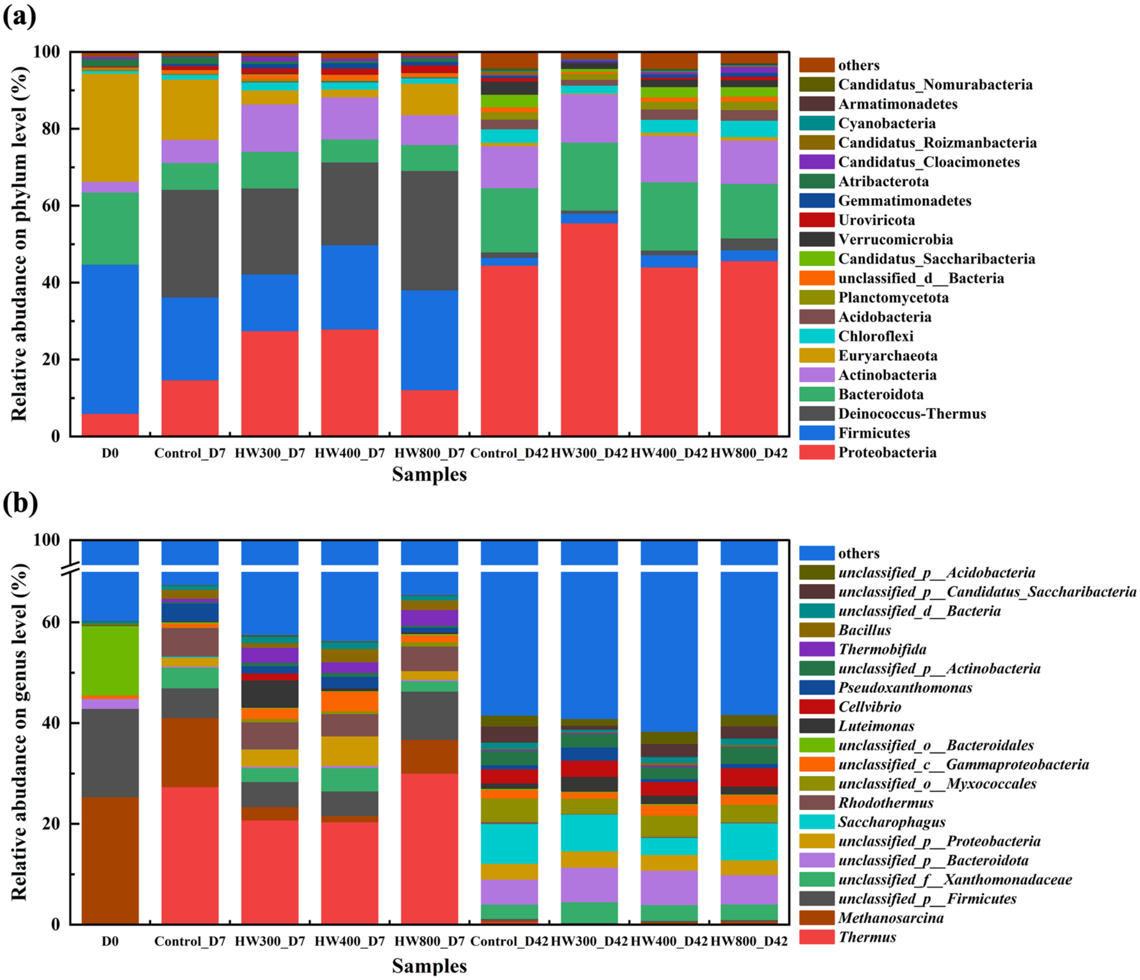

Fig. 5 Comparison of microbial diversity at phylum level (**a**) and genus level (**b**) in composting of food waste digestate amended with hardwood biochar prepared at 300 °C (R2), 400 °C (R3), and 800 °C (R4) against Control (R1)

(26.75%), and Atribacterota (1.9%). Subsequent samples collected on day 7 reflected microbial activity during the thermophilic phase. As the composting progressed and temperature increased, Proteobacteria (mean: 20.09%) exhibited a higher abundance compared to day 0, while Firmicutes maintained a relatively stable composition (mean: 22.99%). Deinococcus-Thermus exhibited a dramatic increase in relative abundance, reaching a mean abundance (24.9%) comparable to that of other major phyla on day 7, possibly owing to its resilience to high temperatures (Araujo et al. 2021). Correspondingly, the abundance of Bacteroidota dropped from 17.07% on day 0 to a mean of 6.71% on day 7 (representing a 2.5-fold decrease). This decline, consistent with the typical thermophilic succession reported by Fang et al. (2023), reflects the suppression of these mesophilic bacteria under high temperatures and a functional shift toward degrading more recalcitrant materials. In comparison with the Control treatments, the addition of biochar led to a decrease in the abundance of Euryarchaeota, possibly due to improved aeration facilitated by biochar (Araujo et al. 2021). Toward the end of composting, as the temperature decreased and stabilized, the abundance of Proteobacteria rebounded, while Bacteroidota, Chloroflexi, Candidatus_Cloacimonetes, Planctomycetota, and Verrucomicrobia increased (Bello et al. 2020; Gurmessa et al. 2021). Deinococcus-Thermus and Firmicutes exhibited a significant decrease. At maturity (day 42), trend analysis of phylum-level relative abundances indicated that microbial community composition was comparable among treatments at the end of composting ($p \geq 0.05$). Of note, the HW300 treatment showed a numerically elevated abundance of Proteobacteria (54.0%) relative to the Control (42.6%), a trend consistent with literature on biochar effects (Xiong et al. 2021, 2023), though this inter-treatment difference with Control was not statistically significant ($p \geq 0.05$) at the phylum level.

At the genus level (Fig. 5b), notable variations were observed in the microbial communities across different composting periods. The methanogenic archaeon *Methanosarcina* (24%) constituted the predominant genus, a direct reflection of its anaerobic origin in the FWD feedstock, followed by *unclassified_p__Firmicutes* (16.01%), *unclassified_o__Bacteroidales* (11.82%), and *unclassified_p__Bacteroidota* (1.7%) (Liu et al. 2016). Over the course of composting, microbial succession occurred, leading to a reduction in the abundance of *Methanosarcina*, consistent with the shift to aerobic conditions. Additionally, the presence of *Methanosarcina* was lower in biochar-amended treatments compared to the Control treatments, possibly due to enhanced aeration facilitated by hardwood biochar but no significant difference among treatments amended by biochar produced at different temperatures. The abundance of unclassified Firmicutes also decreased, which usually has higher abundance during the thermophilic phase, as found in studies by Daims et al. (2016). *Thermus*, *unclassified_p__Proteobacteria*, *unclassified_f__Xanthomonadaceae*, *Rhodothermus*, *Pseudoxanthomonas*, *Bacillus*, *Thermobifida* emerged during the high temperature phases of composting (Araujo et al. 2021; Beffa et al. 1996; Fang et al. 2023; Partanen et al. 2010). Both HW300 and HW400 enriched some genera of Proteobacteria. Since most nitrifiers belong to the Proteobacteria phylum, the higher nitrification observed in the composting amended by HW300 and HW400 led to increased levels of NO_2^- and NO_3^-. Toward the end of composting, microbial diversity increased with decrease in temperatures, and mesophiles were observed to be more prevalent. *Unclassified_p__Bacteroidota* recovered, and *Saccharophagus*, *unclassified_o__Myxococcales*, *unclassified_p__Actinobacteria*, *Cellvibrio*, *unclassified_p__Candidatus_Saccharibacteria*, and *unclassified_p__Acidobacteria* demonstrated increased relative abundance (Wang et al. 2022). However, *Thermus*, *Methanosarcina*, *unclassified_p__Firmicutes*, *Rhodothermus*, and *Thermobifida* thermophilic microbes were not detected (Wen et al. 2021).

3.5.2 Nitrogen-related microbial community

The nitrifiers community was investigated by focusing on genera prefixed with 'Nitro-', thereby capturing the majority of canonical chemolithoautotrophic nitrifiers (AOB and NOB). Key nitrogen-metabolizing genera identified included *Nitrosospira*, *Nitrosomonas*, *Nitrosovibrio*, and *Nitratireductor* (Table 2); these genera are commonly found in the chicken manure, kitchen cattle manure, and poultry manure composting (Ding et al. 2019; Ma et al. 2022; Posmanik et al. 2014; Sun et al. 2019). By day 7, most of the nitrifiers had increased and *Nitrososphaera* exhibited higher abundance in biochar-amended treatments compared to the Control treatments. AOB, such as *Nitrosomonas*, *Nitrosospira*, *Nitrosovibrio*, *unclassified_Nitrosomonadales*, *Nitrosococcus*, and Archaea such as *Nitrosopumilus* and *Nitrososphaera*, play a role in the initial steps of nitrification converting NH_3 to NO_2^- in the initial phase of nitrification. Biochar-amended treatments showed higher reads for both AOB and NOB compared to the Control. For instance, AOB reads were 5988 (HW300), 12,522 (HW400), and 3882 (HW800), versus 2512 in the Control (Xie et al. 2012; Yan et al. 2018). Additionally, genus for NOB favoring oxidation of NO_2^- to NO_3^-, such as *Nitrobacter*, *Nitrococcus*, *Nitrolancea*, *Nitrospira*, *unclassified_Nitrospiraceae*, *unclassified_Nitrospinae*, and *unclassified_Nitrospira*, were higher in biochar-amended treatments than in the Control, with 14,540 (HW300), 17,584 (HW400), and 12,196 (HW800) reads (Fujitani et al. 2014; Pérez et al. 2015). Total nitrifier reads were also higher in biochar treatments (HW300: 20,528; HW400: 30,106; HW800: 16,078) than in the Control (10,600), correlating with elevated NO_2^- and NO_3^- levels and indicating that biochar promoted nitrifier growth. This promotion may be attributed to an earlier temperature drop in biochar treatments, likely due to faster organic matter consumption or improved oxygen transfer, which initiated nitrification earlier. By the end of composting, the abundance of genera like *Nitrosospira*, *Nitrobacter*, and *Nitrosovibrio* in the Control caught up with that in biochar treatments, possibly due to earlier NH_4^+-N depletion in the latter.

Among the dominant genera, *Nitratireductor* and *Denitrificimonas* have denitrification potential and have been recognized as nitrifiers and denitrifiers in manure composting and denitrification systems (He et al. 2021; Saati-Santamaría et al. 2021; Zhang et al. 2023). Their detection during the thermophilic phase suggests N_2O was likely produced mainly through denitrification and nitrification–denitrification coupling. Subsequent growth of autotrophic AOB may have introduced an aerobic N_2O emission pathway. Therefore, elucidating NH_3 and N_2O emission mechanisms requires integrating environmental factors like oxygen content (Zhu et al. 2013).

3.5.3 Analysis of nitrogen metabolic pathway

The functional potential inferred from the KEGG nitrogen metabolism pathway (ko00910) provides a mechanistic explanation for the observed trade-off between NH_3 and N_2O emissions (Tian et al. 2023; Xiong et al. 2022). The best NH_3 mitigation by HW300 (Fig. 3e) coincided with its higher inferred abundance of genes encoding hydroxylamine oxidase [EC:1.7.2.6], particularly during the curing phase (Fig. 6a), indicating enhanced

Table 2 Microbial diversity associated with nitrogen transformation in food waste digestate compost amended with biochar

Phylum	Class	Genus	Groups (reads abundance)									
			D0	Day 7				Day 42				Total
				Control	HW300	HW400	HW800	Control	HW300	HW400	HW800	
Proteobacteria	Alphaproteobacteria	*Nitratireductor*	596	6620	13,820	7596	7546	19,946	13,298	14,330	17,682	101,434
		Nitrobacter	250	500	1802	1222	764	3472	1644	1628	1366	12,648
	Betaproteobacteria	*Nitrosomonas*	500	804	2148	2390	1468	11,958	13,538	17,786	16,596	67,188
		Nitrosospira	36	236	942	2382	586	53,322	22,598	20,202	35,496	135,800
		Nitrosovibrio	0	528	412	956	146	19,526	7840	7512	12,694	49,614
		Unclassified _Nitrosomonadales	120	196	898	1060	342	3590	2726	3098	2698	14,728
	Gammaproteobacteria	*Nitrococcus*	70	404	870	3482	870	756	472	618	880	8422
		Nitrosococcus	346	500	772	4462	446	1028	716	1664	1172	11,106
		Denitrificimonas	3818	74	524	70	88	52	76	16	28	4746
Chloroflexi	Thermomicrobia	*Nitrolancea*	70	1112	3232	2882	2830	1346	678	1246	2282	15,678
Nitrospirae	Nitrospira	*Nitrospira*	294	760	2388	2220	1440	10,630	3370	7490	9034	37,626
		Unclassified _Nitrospiraceae	3622	2064	1574	1328	1604	2294	1182	1744	2262	17,674
Nitrospinae	Unclassified _Nitrospinae	*Unclassified _Nitrospinae*	240	834	1184	1712	1198	1486	668	1404	1628	10,354
Nitrospirae	Unclassified _Nitrospirae	*Unclassified _Nitrospirae*	2266	2414	3490	4738	3490	4848	2056	4870	5434	33,606
Thaumarchaeota	Unclassified _Thaumarchaeota	*Nitrosopumilus*	0	32	50	92	112	5190	212	498	2534	8720
	Nitrososphaeria	*Nitrososphaera*	18	216	766	1180	782	3216	300	1108	1552	9138

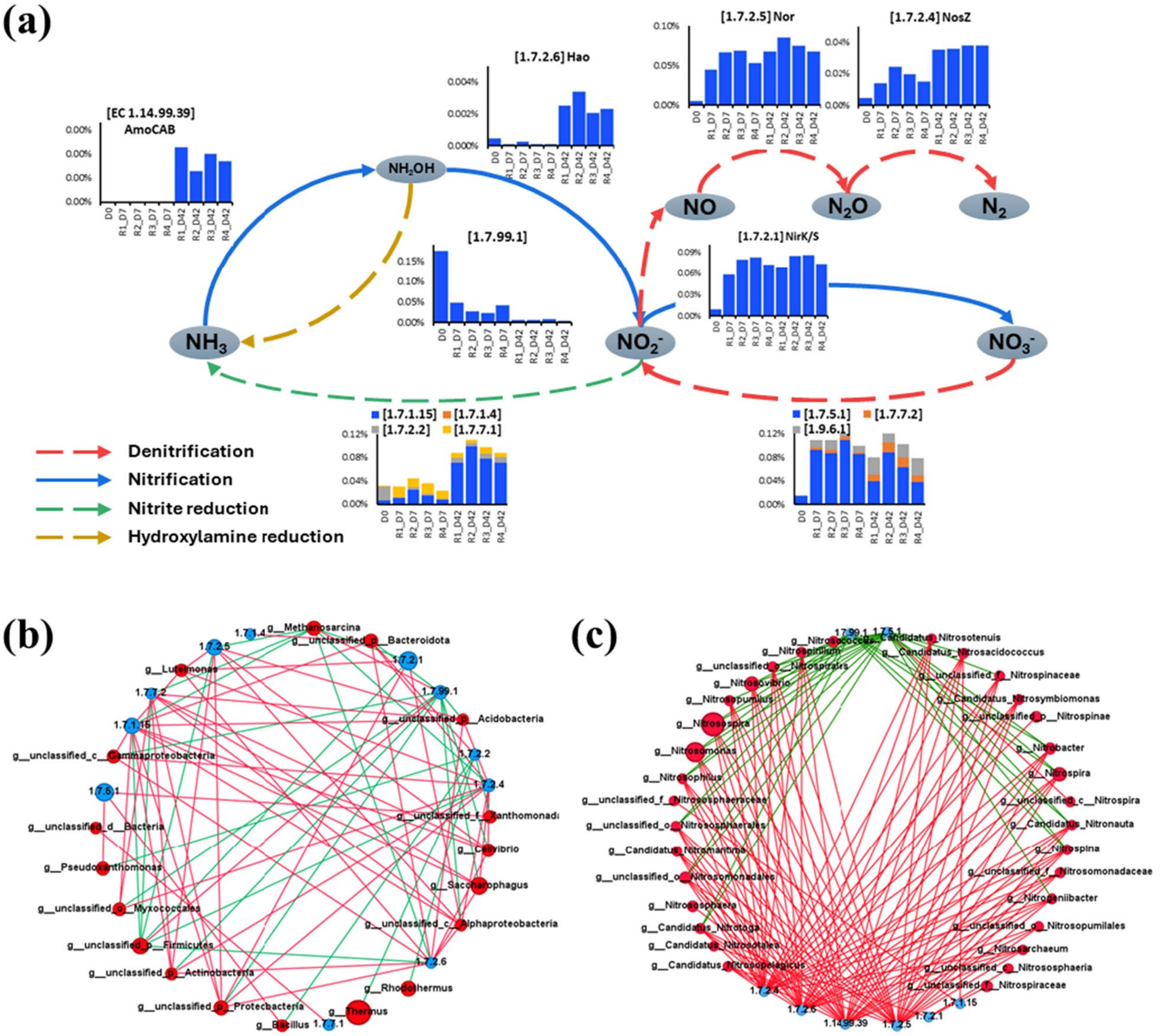

Fig. 6 Metabolic pathway analysis of ko00910 pathway in the overall compost samples. Differences of nitrogen metabolism enzymes and pathway (ko00910) between groups based on Kyoto Encyclopedia of Genes and Genomes (KEGG) database (**a**). Network analysis of enzyme (ko00910)-dominant genus interactions (**b**). Positive correlations are shown in red, and negative in green, with a threshold correlation coefficient: 0.5 and *p*-value < 0.05. Node size indicates the degree of connectivity. Network analysis of enzyme (ko00910)-dominant nitrifiers interactions (**c**). Positive correlations are shown in red, and negative in green, with a threshold correlation coefficient: 0.5 and *p*-value < 0.05. Node size indicates the degree of connectivity

nitrification that converted NH_4^+ into NO_3^-, thereby reducing the substrate pool for NH_3 volatilization.

Conversely, the trade-off in N_2O emissions was mirrored in the denitrification genetic potential. HW300, which exhibited the highest cumulative N_2O emission among biochar treatments (Fig. 3g), showed elevated abundances of genes encoding nitrite reductase (NO-forming) [EC:1.7.2.1] (*nirK*/*nirS*), nitric oxide reductase [EC:1.7.2.5] (*nor*), and nitrate reductase [EC:1.7.5.1; 1.7.7.2] (*narG*/*napA*), particularly during the curing phase (Fig. 6a). However, the relative abundance of genes for nitrous-oxide reductase [EC:1.7.2.4] (*nosZ*) in the HW300 treatment did not increase proportionally. This imbalance within the denitrification cascade (higher abundance of *nirK/S* & *nor* vs. *nosZ*) likely contributed to its higher N_2O emission potential of HW300 treatment. The elevated NO_2^- concentration in HW300 (Fig. 3b) likely further fueled this pathway. In contrast, HW800, which achieved the greatest N_2O reduction, was associated with a microbial community exhibiting lower overall

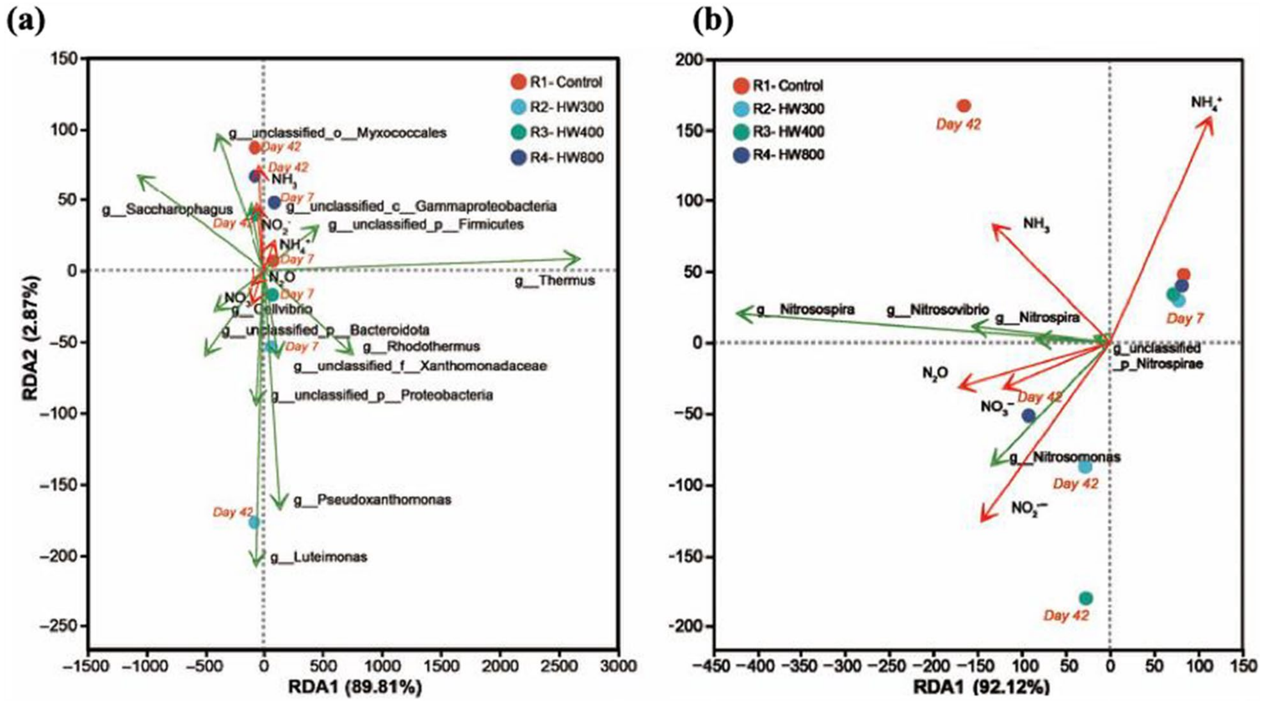

Fig. 7 Redundancy analysis (RDA) of bacterial community structure in relation to nitrogen-related environmental factors: (**a**) microbial taxa annotated to the nitrogen metabolism pathway (ko00910); (**b**) core nitrifiers

denitrification potential (Fig. 6a). The low abundance of upstream denitrification genes (e.g., *narG*/*napA*, which are sensitive to oxygen availability) suggests limited initiation of the denitrification cascade, aligning with its well-aerated microporous structure that minimizes anaerobic niches.

Notably, HW400 presented an intermediate and optimal profile. It maintained substantial nitrification potential (supporting NH_3 mitigation) while exhibiting a less pronounced imbalance in the denitrification gene repertoire compared to HW300. The *nosZ* activity relative to upstream *nirK*/*nirS* and *nor* genes was more favorable in HW400 than in HW300 (Fig. 6a), which likely contributed to its lower N_2O emissions compared to HW300 and its optimal overall nitrogen conservation.

Within the microbial community of FWD composting, the correlation between key enzymes determined by the ko00910 pathway and dominant genera was revealed. Genera such as *g__Saccharophagus*, *g__unclassified_p__Proteobacteria*, *g__unclassified_p__Bacteroidota*, and *g__Cellvibrio* exhibited significant positive associations with denitrifying enzyme activity. Conversely, genera such as *g__Pseudoxanthomonas*, *g__unclassified_f__Xanthomonadaceae*, and *g__Bacillus* showed close positive correlations with the most active [EC 1.7.5.1] enzyme activity. Additionally, genera such as *g__unclassified_p__Proteobacteria*, *g__Luteimonas*, and *g__unclassified_c__Alphaproteobacteria* demonstrated significant positive correlations with *nirK/S* activity [EC 1.7.2.1]. The top three genera highly positively correlated with [EC 1.7.2.5] nitric oxide reductase (*nor*) activity were *g__Cellvibrio*, *g__Luteimonas*, and *g__unclassified_c__Alphaproteobacteria*. Furthermore, *g__unclassified_c__Alphaproteobacteria* and *g__unclassified_p__Acidobacteria* exhibited a high correlation with *nosZ* activity (correlation value of 0.9, $p < 0.05$) (Fig. 6b). The consistent, positive correlations between genera *Luteimonas*, *Cellvibrio* and enzymes for *nirK/S* [EC 1.7.2.1 and *nor* [EC 1.7.2.5] define a core module for incomplete denitrification. The significant enrichment of these correlated genera in the HW300 treatment (Fig. 5b) suggests this module was functionally amplified, mechanistically explaining the higher N_2O emission potential observed. The abundance of major nitrifiers correlate significantly ($p < 0.05$) positively with nitrification enzymes [EC 1.7.2.6] and [EC 1.14.99.39]. Moreover, they also show positive associations with denitrification enzymes such as [EC1.7.21] *nirK/S*, [EC 1.7.2.4] *nor*, and [EC 1.7.2.5] *nosZ*, while all the nitrifying genera exhibit negative correlations with denitrifiers enzymes such as [EC 1.7.99.1] and [EC 1.7.5.1]. Key genera determined by the most nodes and abundance in nitrogen transformation include AOB *Nitrosomonas* and *Nitrosospira*, as well as NOB *Nitrobacter* and *Nitrospira*

(Fig. 6c). The early enrichment of these key genera in biochar treatments (Table 2) probably reinforced their cooperative network (Fig. 6c), which in turn drove efficient nitrification.

3.5.4 Relationships between nitrogen-cycling microbial communities and environmental factors

Redundancy analysis (RDA) conducted at the genus level explained 92.68% of the cumulative variance in the bacterial community structure associated with the nitrogen pathway, with RDA1 contributing 89.81% and RDA2 contributing 2.87% (Fig. 7a). Permutation tests indicated that NO_3^- ($p = 0.006$) and N_2O ($p = 0.028$) were statistically significant environmental drivers, whereas NH_3, NH_4^+, and NO_2^- were not significant ($p \geq 0.05$). The RDA loadings showed that NO_3^- (loading = −0.975) and N_2O (loading = −0.996) were strongly negatively correlated with RDA1, while NH_4^+ was positively correlated with RDA1 (loading = +0.978). In the ordination plot, several genera and unclassified genus-level taxa were positioned close to the NO_3^- and N_2O vectors, suggesting a positive association with these variables. These included the genera *Luteimonas*, *Pseudoxanthomonas*, and *Cellvibrio*, as well as unclassified taxa within the phyla Proteobacteria (*g__unclassified_p__Proteobacteria*) and Bacteroidota (*g__unclassified_p__Bacteroidota*). Among these, *Cellvibrio* exhibited near-parallel alignment with the N_2O vector, indicating a strong positive correlation, while the greater arrow length for *Luteimonas* implied a comparatively stronger influence on N_2O emission. These results highlight the distinct responses of different bacterial genera to nitrogen-related environmental gradients, with NO_3^- and N_2O serving as key explanatory variables in the RDA model. The RDA model applied to the key nitrifiers showed enhanced explanatory power, with the first two RDA axes explaining 95.48% of the cumulative variance (RDA1: 92.12%, $p < 0.001$; RDA2: 3.36%, $p < 0.05$). Permutation tests identified NH_4^+ ($p = 0.004$, RDA1 loading = 0.669) and NO_3^- ($p = 0.022$, RDA1 loading = −0.812) as the dominant and statistically significant environmental drivers, while N_2O was also significant ($p = 0.046$, RDA1 loading = −0.981) (Fig. 7b). Specifically, canonical AOB such as *Nitrosospira*, *Nitrosomonas*, and *Nitrosovibrio* were strongly negatively correlated with NH_4^+ concentration (as indicated by their opposing positions along RDA1) and positively correlated with NO_2^- and NO_3^- levels. Among these AOB, *Nitrosospira* appeared to be the most influential genus in driving nitrogen conversion. In contrast, NOB including *Nitrospira* were spatially positioned closer to the NO_3^- vector (RDA1 loading = −0.812), consistent with their metabolic role.

The contrasting nitrogen conservation outcomes can be attributed to the distinct micro-environments shaped by biochars of different pyrolysis temperatures, with HW400 achieving an optimal balance. The HW300 biochar, with its abundant oxygen-containing functional groups (Fig. 1d), is proposed to have NH_4^+-enriched micro-sites that possible fostered the enrichment of AOB, (e.g., *Nitrosomonas*), thereby accelerating nitrification and reducing NH_3 volatilization. However, this same microenvironment, coupled with its limited porosity, may have promote incomplete denitrification by enriching *nirK*/*nirS*-harboring denitrifiers (e.g., *Luteimonas*), leading to higher N_2O emissions. Conversely, HW800, characterized by high surface area and a better-developed, often microporous structure (Table 1, Fig. 1), likely enhanced oxygen diffusion and minimized persistent anaerobic niches. This appears to have suppressed denitrifier activity, resulting in the greatest N_2O reduction but offering limited enhancement to nitrification and overall nitrogen retention. The evidence therefore points to HW400's exhibiting an optimal property combination that harmonized these opposing effects. Its intermediate pore structure (Table 1) presumably facilitated adequate oxygen supply to suppress dominant N_2O-producing denitrifiers, while its retained functional groups and higher CEC would have ensured sufficient NH_4^+ retention and bioavailability to support a robust nitrifier community. Consequently, HW400 is inferred to have orchestrated a microbial consortium that concurrently facilitated efficient nitrification (reducing NH_3 loss) and minimized N_2O production, leading to the highest net nitrogen conservation.

It is acknowledged that these mechanistic links, while strongly supported by correlative data, are inferred. Future studies employing targeted techniques such as quantitative PCR (qPCR) for key functional genes (e.g., *amoA*, *nirK*/*nirS*, *nosZ*) across specific composting phases would provide direct validation of the proposed microbial mechanisms.

3.6 Practical implications, policy support, and future perspectives

The scalability and economic viability of this optimized biochar strategy are supported by well-defined technical parameters and its alignment with a mature, scalable pyrolysis technology at 400 °C, which avoids the extreme energy demands of higher temperatures (Karunarathna et al. 2025). Utilizing hardwood waste, a globally abundant residue, ensures broad applicability and sustainable feedstock supply. While a precise techno-economic assessment requires future pilot-scale validation, the direct benefits identified in this study, including enhanced nitrogen retention (improving compost fertilizer value) and substantial reduction of the potent greenhouse gas N_2O and NH_3, demonstrate clear economic and environmental value. Widespread adoption would be further accelerated by policy frameworks that internalize these environmental externalities, such as mature carbon markets and incentives for high-quality, carbon-sequestering soil amendments.

Beyond the direct process economics, the long-term agronomic and environmental value of the final product further strengthens the case for such policy support. The biochar-compost product promises long-term soil benefits: persistent carbon sequestration from the stable biochar, reduced nutrient leaching via its adsorption properties, and the introduction of a nitrifier-enriched microbial community to potentially enhance soil nitrogen cycling. These agronomic and environmental co-benefits reinforce its value as a multifunctional soil amendment (Mikajlo et al. 2024).

It should be noted that the conclusions of this study are derived from lab-scale experiments using a specific hardwood biochar and food waste digestate in duplicate reactors (n = 2 per treatment), a setup typical for controlled mechanistic studies but that limits robust statistical inference. Therefore, our findings are based on clear, consistent trends across treatments, and the identified optimal pyrolysis temperature (400 °C) and associated microbial responses may vary with other feedstocks or operational scales. Future work should prioritize validation under pilot- or full-scale conditions with increased replication, coupled with detailed techno-economic analysis, to rigorously assess practical scalability.

4 Conclusions

This study, conducted at a fixed biochar addition rate of 10% (dry weight), demonstrates that pyrolysis temperature governs the properties of hardwood biochar, thereby directing nitrogen transformation during FWD composting through selective regulation of microbial community structure. Biochar produced at 300 °C, with its abundant functional groups, enhanced ammonium adsorption and enriched AOB (e.g., *Nitrosomonas*), leading to a 39.2% reduction in NH_3 emissions (vs. control, n = 2, $p < 0.05$). However, HW300 also appeared to stimulated the growth of denitrifiers harboring *nirK* and *nirS* genes (e.g., *Luteimonas*), which could have resulted in an imbalance between nitrite reductase and nitrous oxide reductase activity and consequently increased N_2O emission potential. In contrast, HW800 exhibited high porosity, a property correlated with improved oxygen availability, and lower denitrifiers activity, achieving a 47.5% reduction in N_2O emissions (vs. control, n = 2, $p < 0.05$), though with limited overall nitrogen retention. Notably, HW400 established an optimal balance. The resulting microbial community was associated with both efficient nitrification and enhanced N_2O reduction, ultimately reducing total nitrogen loss by 46.3% (vs. control, n = 2, $p < 0.05$). These findings underscore that hardwood biochar functions not merely as an adsorbent but as an ecological driver shaping microbial communities involved in nitrogen metabolism. Pyrolysis temperature can thus be optimized to steer the microbial community structure—specifically the balance between AOB, NOB, and denitrifiers, toward desired nitrogen conservation outcomes. Future research should explore biochar functionalization strategies aimed at selectively enriching beneficial nitrifiers while enhancing the activity of N_2O-reducing microorganisms, providing a targeted approach to optimize nitrogen management during composting.

Supplementary Information

The online version contains supplementary material available at https://doi.org/10.1007/s42773-026-00588-x.

Supplementary Material 1.

Acknowledgements
The authors extend the sincere thanks to Opark 1 for providing the food waste digestate. The insightful discussions and support from all colleagues are deeply appreciated.

Author contributions

Dongyi Li was responsible for the experimental work, including material preparation, data collection, analysis, and writing the original draft. Jonathan W.C. Wong provided overall supervision and managed the project. Jun Zhou, Jialin Liang, Quixiang Xu, Jiayu Zhang, Wenhua Xue participated in the study's conception and design, reviewed the manuscript, and all the authors approved the final version.

Funding
The research leading to these results received funding from the Guangdong Regional Joint Fund (Grant No. 2024A1515110159), the Dongguan University of Technology Top Talent Professor Start-up Fund (No. 221110133), and the Talent Startup Fund (No. 221110356005).

Data availability

The datasets used or analyzed during the current study are available from the corresponding author upon reasonable request.

Declarations

Competing interests

The authors have no relevant financial or non-financial interests to disclose.

Author details
[1]Research Center for Eco-Environmental Engineering, Dongguan University of Technology, Dongguan 523808, Guangdong, China. [2]Bioenergy Research Institute, College of Biotechnology and Pharmaceutical Engineering, Nanjing Tech University, Nanjing 211816, Jiangsu, China. [3]College of Resources and Environment, Zhongkai University of Agriculture and Engineering, Guangzhou 510225, Guangdong, China.

Received: 19 October 2025 Revised: 24 January 2026 Accepted: 28 January 2026

References

Adesemuyi MF, Adebayo MA, Akinola AO, Olasehinde EF, Adewole KA, Lajide L (2020) Preparation and characterisation of biochars from elephant grass and their utilisation for aqueous nitrate removal: effect of pyrolysis temperature. J Environ Chem Eng 8:2213–3437. https://doi.org/10.1016/j.jece.2020.104507

Agyarko-Mintah E, Cowie A, Singh BP, Joseph S, Van-Zwieten L, Cowie A, Harden S, Smillie R (2017a) Biochar increases nitrogen retention and lowers greenhouse gas emissions when added to composting poultry litter. Waste Manage 61:138–149. https://doi.org/10.1016/j.wasman.2016.11.027

Agyarko-Mintah E, Cowie A, Van Zwieten L, Singh BP, Smillie R, Harden S, Fornasier F (2017b) Biochar lowers ammonia emission and improves nitrogen retention in poultry litter composting. Waste Manage 61:129–137. https://doi.org/10.1016/j.wasman.2016.12.009

Ajuna BH, Maung CEH, Kim KYP (2020) Metagenomic analysis reveals enhanced biodiversity and composting efficiency of lignocellulosic waste by thermoacidophilic effective microorganism (tEM). J Environ Manage 276:1095–8630. https://doi.org/10.1016/j.jenvman.2020.111252

Ambaye TG, Vaccari M, Hullebusch EDV, Amrane A, Rtimi S (2020) Mechanisms and adsorption capacities of biochar for the removal of organic and inorganic pollutants from industrial wastewater. Int J Environ Sci Technol 2021:10–13. https://doi.org/10.1007/s13762-020-03060-w

Angnes G, Nicoloso RS, da Silva MLB, de Oliveira PAV, Higarashi MM, Mezzari MP, Miller PRM (2013) Correlating denitrifying catabolic genes with N2O and N2 emissions from swine slurry composting. Bioresour Technol 140:368–375. https://doi.org/10.1016/J.BIORTECH.2013.04.112

Araujo ASF, de Pereira APdA, Antunes JEL, Oliveira LMdS, de Melo WJ, Rocha SMB, do Amorim MR, Araujo FF, et al (2021) Dynamics of bacterial and archaeal communities along the composting of tannery sludge. Environ Sci Pollut Res 28:64295–64306. https://doi.org/10.1007/s11356-021-15585-9

Awasthi MK, Duan YM, Awasthi SK, Liu T, Zhang ZQ (2020) Effect of biochar and bacterial inoculum additions on cow dung composting. Bioresour Technol 297:122407. https://doi.org/10.1016/j.biortech.2019.122407

Azim K, Soudi B, Boukhari S, Perissol C, Roussos S, Thami Alami I (2018) Composting parameters and compost quality: a literature review. Org Agric 8:141–158. https://doi.org/10.1007/s13165-017-0180-z

Balmuk G, Videgain M, Manyà JJ, Duman G, Yanik J (2023) Effects of pyrolysis temperature and pressure on agronomic properties of biochar. J Anal Appl Pyrolysis 169:105858. https://doi.org/10.1016/j.jaap.2023.105858

Beffa T, Blanc M, Marilley L, Fischer JL, Lyon P-F, Aragno M (1996) Taxonomic and metabolic microbial diversity during composting. The Science of Composting. https://doi.org/10.1007/978-94-009-1569-5_16

Bello A, Han Y, Zhu H, Deng L, Yang W, Meng Q, Sun Y, Egbeagu UU et al (2020) Microbial community composition, co-occurrence network pattern and nitrogen transformation genera response to biochar addition in cattle manure-maize straw composting. Sci Total Environ 721:137759–137759. https://doi.org/10.1016/j.scitotenv.2020.137759

Buchfink B, Xie C, Huson DH (2015) Fast and sensitive protein alignment using DIAMOND. Nat Methods 12:59–60. https://doi.org/10.1038/nmeth.3176

Cáceres R, Malińska K, Marfà O (2018) Nitrification within composting: a review. Waste Manag 72:119–137. https://doi.org/10.1016/j.wasman.2017.10.049

Cantrell KB, Hunt PG, Uchimiya M, Novak JM, Ro KS (2012) Impact of pyrolysis temperature and manure source on physicochemical characteristics of biochar. Bioresour Technol 107:419–428. https://doi.org/10.1016/j.biortech.2011.11.084

Cole EJ, Zandvakili OR, Xing B, Hashemi M, Herbert S, Mashayekhi HH (2019) Dataset on the effect of hardwood biochar on soil gravimetric moisture content and nitrate dynamics at different soil depths with FTIR analysis of fresh and aged biochar. Data Brief 25:2352–3409. https://doi.org/10.1016/j.dib.2019.104073

Daims H, Lücker S, Wagner M (2016) A new perspective on microbes formerly known as nitrite-oxidizing bacteria. Trends Microbiol 24:699–712. https://doi.org/10.1016/j.tim.2016.05.004

Dar RA, Dai B, Tsui T-H, Zhang X, Zhang D, Zhou P, Liu R, Zhang L (2025) Bioaugmentation with a lipid-degrading bacterial culture to enhance methane production from food waste anaerobic digestion: effect on process performance, microbial dynamics, and lipid metabolism. Chem Eng J 518:1385–8947. https://doi.org/10.1016/j.cej.2025.164539

Deng L, Liu W, Chang N, Sun L, Zhang J, Bello A, Uzoamaka Egbeagu U, Shi S et al (2023) Disentangling the coupling relationships between functional denitrifiers and nitrogen transformation during cattle-manure and biochar composting: A novel perspective. Bioresour Technol 367:0960–8524. https://doi.org/10.1016/j.biortech.2022.128235

Ding Y, Wei J, Xiong J, Zhou B, Cai H, Zhu W, Zhang H (2019) Effects of operating parameters on in situ NH_3 emission control during kitchen waste composting and correlation analysis of the related microbial communities. Environ Sci Pollut Res 26:11756–11766. https://doi.org/10.1007/s11356-019-04605-4

Fang T, Wang T, Zhao M, Bai L, Deng Y, Ruan W (2023) Food waste digestate composting enhancement by sodium polyacrylate addition: effects on nitrogen transformation processes and bacterial community dynamics. J Environ Manage 325:0301-4797. https://doi.org/10.1016/j.jenvman.2022.116531

Fu L, Niu B, Zhu Z, Wu S, Li W (2012) CD-HIT: accelerated for clustering the next-generation sequencing data. Bioinformatics 28:3150–3152. https://doi.org/10.1093/bioinformatics/bts565

Fu T, Shangguan H, Wei J, Wu J, Tang J, Zeng RJ, Zhou S (2022) In-situ electrolytic oxygen is a feasible replacement for conventional aeration during aerobic composting. J Hazard Mater 426:0304-3894. https://doi.org/10.1016/j.jhazmat.2021.127846

Fu X, Zuo H, Wang Z, Shang P, Li Z, Li J, Zhan Y, Wang Q et al (2025) Extreme thermophilic microbial inoculation for reducing NH3 and N_2O emissions in hyperthermophilic aerobic composting of refinery waste activated sludge. J Environ Manage 380:124870. https://doi.org/10.1016/j.jenvman.2025.124870

Fujitani H, Ushiki N, Tsuneda S, Aoi Y (2014) Isolation of sublineage I *Nitrospira* by a novel cultivation strategy. Environ Microbiol 16:3030–3040. https://doi.org/10.1111/1462-2920.12248

Fukumoto Y, Suzuki K, Osada T, Kuroda K, Hanajima D, Yasuda T, Haga K (2006) Reduction of nitrous oxide emission from pig manure composting by addition of nitrite-oxidizing bacteria. Environ Sci Technol 40:6787–6791. https://doi.org/10.1021/ES0611801

Gao Y, Mania D, Mousavi SA, Lycus P, Arntzen M, Woliy K, Lindström K, Shapleigh JP et al (2021) Competition for electrons favours N_2O reduction in denitrifying *Bradyrhizobium* isolates. Environ Microbiol 23:2244–2259. https://doi.org/10.1111/1462-2920.15404

Gurmessa B, Milanovic V, Foppa Pedretti E, Corti G, Ashworth AJ, Aquilanti L, Ferrocino I, Rita Corvaglia M et al (2021) Post-digestate composting shifts microbial composition and degrades antimicrobial resistance genes. Bioresour Technol 340:0960–8524. https://doi.org/10.1016/j.biortech.2021.125662

Hagemann N, Joseph S, Schmidt HP, Kammann CI, Harter J, Borch T, Young RB, Varga K et al (2017) Organic coating on biochar explains its nutrient retention and stimulation of soil fertility. Nat Commun 8:1089. https://doi.org/10.1038/s41467-017-01123-0

He X, Yin H, Fang C, Xiong J, Han L, Yang Z, Huang G (2021) Metagenomic and q-PCR analysis reveals the effect of powder bamboo biochar on nitrous oxide and ammonia emissions during aerobic composting. Bioresour Technol 323:124567. https://doi.org/10.1016/J.BIORTECH.2020.124567

He X, Yin H, Han L, Cui R, Fang C, Huang G (2019) Effects of biochar size and type on gaseous emissions during pig manure/wheat straw aerobic composting: insights into multivariate-microscale characterization and microbial mechanism. Bioresour Technol 271:375–382. https://doi.org/10.1016/j.biortech.2018.09.104

Hoseini M, Cocco S, Casucci C, Cardelli V, Ruello ML, Serrani D, Corti G (2025) Producing agri-food derived composts from coffee husk as primary feedstock at different temperature conditions. J Environ Manage 373:0301-4797. https://doi.org/10.1016/j.jenvman.2024.123485

Hu X, Zhang X, Ngo HH, Guo W, Wen H, Li C, Zhang Y, Ma C (2020) Comparison study on the ammonium adsorption of the biochars derived from different kinds of fruit peel. Sci Total Environ 707:0048-9697. https://doi.org/10.1016/j.scitotenv.2019.135544

Huang W, Sun X, Sun H, Feng Y, Gong X, Ma Y, Jiang J, Xue L (2024) Effects of biochar and wood vinegar co-application on composting ammonia and nitrous oxide losses and fertility. Bioresour Technol 412:131388. https://doi.org/10.1016/j.biortech.2024.131388

Hyatt D, Chen G-L, Locascio PF, Land ML, Larimer FW, Hauser LJ (2010) Prodigal: prokaryotic gene recognition and translation initiation site identification. BMC Bioinformatics 11:119. https://doi.org/10.1186/1471-2105-11-119

Janczak D, Malińska K, Czekała W, Cáceres R, Lewicki A, Dach J (2017) Biochar to reduce ammonia emissions in gaseous and liquid phase during composting of poultry manure with wheat straw. Waste Manag 66:36–45. https://doi.org/10.1016/j.wasman.2017.04.033

Kalina M, Sovova S, Svec J, Trudicova M, Hajzler J, Kubikova L, Enev V (2022) The effect of pyrolysis temperature and the source biomass on the properties of biochar produced for the agronomical applications as the soil conditioner. Materials 15:8855. https://doi.org/10.3390/ma15248855

Karunarathna S, Gunasekara C, Law D, Jayathilakage R, Setunge S, Xavier L (2025) Timber and wood waste biochar in cementitious composites: a circular economy approach to performance and sustainability: a review. J Mater Cycles Waste Manag 27:3196–3221. https://doi.org/10.1007/s10163-025-02345-x

Li D, Liu CM, Luo R, Sadakane K, Lam TW (2015a) MEGAHIT: an ultra-fast single-node solution for large and complex metagenomics assembly via succinct de Bruijn graph. Bioinformatics 31:1674–1676. https://doi.org/10.1093/bioinformatics/btv033

Li D, Manu MK, Varjani S, Wong JWC (2023) Role of tobacco and bamboo biochar on food waste digestate co-composting: nitrogen conservation, greenhouse gas emissions, and compost quality. Waste Manag 156:44–54. https://doi.org/10.1016/j.wasman.2022.10.022

Li R, Wang Q, Zhang Z, Zhang G, Li Z, Wang L, Zheng J (2015b) Nutrient transformation during aerobic composting of pig manure with biochar prepared at different temperatures. Environ Technol (United Kingdom) 36:815–826. https://doi.org/10.1080/09593330.2014.963692

Li R, Yu C, Li Y, Lam TW, Yiu SM, Kristiansen K, Wang J (2009) SOAP2: an improved ultrafast tool for short read alignment. Bioinformatics 25:1966–1967. https://doi.org/10.1093/bioinformatics/btp336

Liao J, Hu A, Zhao Z, Liu X, Jiang C, Zhang Z (2021) Biochar with large specific surface area recruits N_2O-reducing microbes and mitigate N_2O emission. Soil Biol Biochem. https://doi.org/10.1016/j.soilbio.2021.108212

Liu C, Li H, Zhang Y, Si D, Chen Q (2016) Evolution of microbial community along with increasing solid concentration during high-solids anaerobic digestion of sewage sludge. Bioresour Technol 216:87–94. https://doi.org/10.1016/j.biortech.2016.05.048

Liu J, Hu Y, Gu S, Li X, Ji Z, Qin H, Zhang L, Zhang J et al (2024) Insight into mitigation mechanisms of N_2O emission by biochar during agricultural waste composting. Bioresour Technol 406:130970. https://doi.org/10.1016/j.biortech.2024.130970

Liu Y, He Z, Uchimiya M (2015) Comparison of biochar formation from various agricultural by-products using FTIR spectroscopy. Mod Appl Sci 9:1913–1852. https://doi.org/10.5539/mas.v9n4p246

Ma Q, Li Y, Xue J, Cheng D, Li Z (2022) Effects of turning frequency on ammonia emission during the composting of chicken manure and soybean straw. Molecules 27:1–21. https://doi.org/10.3390/molecules27020472

Ma S, Shen Y, Ding J, Cheng H, Zhou H, Ge M, Wang J, Cheng Q et al (2024) Effects of biochar and volcanic rock addition on humification and microbial community during aerobic composting of cow manure. Bioresour Technol 391:129973-129973. https://doi.org/10.1016/j.biortech.2023.129973

Manu MK, Li D, Liwen L, Jun Z, Varjani S, Wong JWC (2021a) A review on nitrogen dynamics and mitigation strategies of food waste digestate composting. Bioresour Technol 334:125032. https://doi.org/10.1016/j.biortech.2021.125032

Manu MK, Wang C, Li D, Varjani S, Wong JWC (2022) Impact of zeolite amendment on composting of food waste digestate. J Clean Prod. https://doi.org/10.1016/J.JCLEPRO.2022.133408

Manu MK, Wang C, Li D, Varjani S, Xu Y, Ladumor N, Lui M, Zhou J et al (2021b) Biodegradation kinetics of ammonium enriched food waste digestate compost with biochar amendment. Bioresour Technol 341:125871. https://doi.org/10.1016/J.BIORTECH.2021.125871

Mikajlo I, Lerch TZ, Louvel B, Hynst J, Zahora J, Pourrut B (2024) Composted biochar versus compost with biochar: effects on soil properties and plant growth. Biochar 6:85. https://doi.org/10.1007/s42773-024-00379-2

Nguyen MK, Lin C, Hoang HG, Bui XT, Ngo HH, Le VG, Tran HT (2023) Investigation of biochar amendments on odor reduction and their characteristics during food waste co-composting. Sci Total Environ 865:0048-9697. https://doi.org/10.1016/j.scitotenv.2022.161128

Nguyen MK, Lin C, Hoang HG, Sanderson P, Dang BT, Bui XT, Nguyen NSH, Vo DVN et al (2022) Evaluate the role of biochar during the organic waste composting process: a critical review. Chemosphere 299:134488-134488. https://doi.org/10.1016/j.chemosphere.2022.134488

Olivera-Begue E, Gonzalez D, Kaal J, Camps-Arbestain M, Sanchez A (2025) Commercial-scale co-composting of wood-derived biochar with source-selected organic fraction of municipal solid waste. Bioresour Technol 431:132595. https://doi.org/10.1016/j.biortech.2025.132595

Parasar BJ, Agarwala N (2025) Unravelling the role of biochar-microbe-soil tripartite interaction in regulating soil carbon and nitrogen budget: a panacea to soil sustainability. Biochar 7:37. https://doi.org/10.1007/s42773-024-00411-5

Partanen P, Hultman J, Paulin L, Auvinen P, Romantschuk M (2010) Bacterial diversity at different stages of the composting process. BMC Microbiol 10:94. https://doi.org/10.1186/1471-2180-10-94

Pérez J, Buchanan A, Mellbye B, Ferrell R, Chang JH, Chaplen F, Bottomley PJ, Arp DJ et al (2015) Interactions of *Nitrosomonas europaea* and *Nitrobacter winogradskyi* grown in co-culture. Arch Microbiol 197:79–89. https://doi.org/10.1007/s00203-014-1056-1

Posmanik R, Gross A, Nejidat A (2014) Effect of high ammonia loads emitted from poultry-manure digestion on nitrification activity and nitrifier-community structure in a compost biofilter. Ecol Eng 62:140–147. https://doi.org/10.1016/j.ecoleng.2013.10.033

Saati-Santamaría Z, Peral-Aranega E, Velázquez E, Rivas R, García-Fraile P (2021) Phylogenomic analyses of the genus *pseudomonas* lead to the rearrangement of several species and the definition of new genera. Biol 10:782. https://doi.org/10.3390/biology10080782

Sahoo SS, Vijay VK, Chandra R, Kumar H (2021) Production and characterization of biochar produced from slow pyrolysis of pigeon pea stalk and bamboo. Cleaner Engineering and Technology 3:100101. https://doi.org/10.1016/J.CLET.2021.100101

Shangguan H, Fu T, Shen C, Mi H, Wei J, Tang J, Zhou S (2022) In situ generated oxygen distribution causes maturity differentiation during electrolytic oxygen aerobic composting. Sci Total Environ 850:157939. https://doi.org/10.1016/j.scitotenv.2022.157939

Song B, Manu MK, Li D, Wang C, Varjani S, Ladumor N, Michael L, Xu Y et al (2021) Food waste digestate composting: feedstock optimization with sawdust and mature compost. Bioresour Technol 341:125759. https://doi.org/10.1016/j.biortech.2021.125759

Sun Y, Zhu L, Xu X, Meng Q, Men M, Xu B, Deng L (2019) Correlation between ammonia-oxidizing microorganisms and environmental factors during cattle manure composting. Rev Argent Microbiol 51:371–380. https://doi.org/10.1016/J.RAM.2018.12.002

Tan Z, Yuan S, Hong M, Zhang L, Huang Q (2020) Mechanism of negative surface charge formation on biochar and its effect on the fixation of soil Cd. J Hazard Mater 384:121370. https://doi.org/10.1016/j.jhazmat.2019.121370

Tang J, Li X, Cui P, Lin J, Jianxiong Zeng R, Lin H, Zhou S (2020) Nitrification plays a key role in N2O emission in electric-field assisted aerobic composting. Bioresour Technol 297:122470. https://doi.org/10.1016/j.biortech.2019.122470

Tian X, Qin W, Zhang Y, Liu Y, Lyu Q, Chen G, Feng Z, Ji G et al (2023) The inoculation of thermophilic heterotrophic nitrifiers improved the efficiency and reduced ammonia emission during sewage sludge composting. Chem Eng J 479:147237. https://doi.org/10.1016/j.cej.2023.147237

TMECC. (2015). The Test Method for the Examination of Composting and Compost. U.S. Composting Council. https://compostingcouncil.org/tmecc/

Tomczyk A, Sokołowska Z, Boguta P (2020) Biochar physicochemical properties: pyrolysis temperature and feedstock kind effects. Rev Environ Sci Biotechnol 19:191–215. https://doi.org/10.1007/s11157-020-09523-3

Wang H, Shao T, Zhou Y, Long X, Rengel Z (2023) The effect of biochar prepared at different pyrolysis temperatures on microbially driven conversion and retention of nitrogen during composting. Heliyon 9:13698. https://doi.org/10.1016/j.heliyon.2023.e13698

Wang N, Huang D, Shao M, Sun R, Xu Q (2022) Use of activated carbon to reduce ammonia emissions and accelerate humification in composting digestate from food waste. Bioresour Technol 347:126701. https://doi.org/10.1016/j.biortech.2022.126701

Wang S, Wang L, Sun Z, Wang S, Shen C, Tang Y, Kida K (2021) Biochar addition reduces nitrogen loss and accelerates composting process by affecting the core microbial community during distilled grain waste composting.

Bioresour Technol 337:125492-125492. https://doi.org/10.1016/j.biortech.2021.125492

Wang X, You G, Liu C, Sun Y (2025) Bioaugmentation strategies in co-composting anaerobically digested food waste with agricultural by-products: enhancing fertilizer quality and microbial communities. Ecotoxicol Environ Saf 290:117539. https://doi.org/10.1016/j.ecoenv.2024.117539

Wen P, Tang J, Wang Y, Liu X, Yu Z, Zhou S (2021) Hyperthermophilic composting significantly decreases methane emissions: insights into the microbial mechanism. Sci Total Environ 784:147179-147179. https://doi.org/10.1016/j.scitotenv.2021.147179

Wu J, Shangguan H, Fu T, Chen J, Tang J, Zeng RJ, Ye W, Zhou S (2021) Alternating magnetic field mitigates N_2O emission during the aerobic composting of chicken manure. J Hazard Mater. https://doi.org/10.1016/j.jhazmat.2020.124329

Xie C, Mao X, Huang J, Ding Y, Wu J, Dong S, Kong L, Gao G et al (2011) KOBAS 2.0: a web server for annotation and identification of enriched pathways and diseases. Nucleic Acids Res 39:W316–W322. https://doi.org/10.1093/nar/gkr483

Xie K, Jia X, Xu P, Huang X, Gu W, Zhang F, Yang S, Tang S (2012) Improved composting of poultry feces via supplementation with ammonia oxidizing archaea. Bioresour Technol 120:70–77. https://doi.org/10.1016/j.biortech.2012.06.029

Xiong J, Ma S, He X, Han L, Huang G (2021) Nitrogen transformation and dynamic changes in related functional genes during functional-membrane covered aerobic composting. Bioresour Technol 332:125087-125087. https://doi.org/10.1016/J.BIORTECH.2021.125087

Xiong J, Su Y, He X, Han L, Guo J, Qiao W, Huang G (2022) Effects of functional-membrane covering technique on nitrogen succession during aerobic composting: metabolic pathways, functional enzymes, and functional genes. Bioresour Technol 354:127205-127205. https://doi.org/10.1016/j.biortech.2022.127205

Xiong J, Zhuo Q, Shi Z, He X, Han L, Huang G (2023) Multivariate and multiscale investigation of ammonia production and emission mechanisms during membrane-covered cattle manure/wheat straw aerobic composting. Chem Eng J 478:147511-147511. https://doi.org/10.1016/j.cej.2023.147511

Yan L, Wang G, Ai S, Huo Z, Wang Y, Gu JD, Wang W (2018) Abundance of ammonia-oxidizing bacteria and archaea under different ventilation strategies during cattle manure composting. J Environ Manage 212:375–383. https://doi.org/10.1016/j.jenvman.2018.02.032

Yin Y, Yang C, Li M, Zheng Y, Ge C, Gu J, Li H, Duan M et al (2021) Research progress and prospects for using biochar to mitigate greenhouse gas emissions during composting: a review. Sci Total Environ 798:149294-149294. https://doi.org/10.1016/j.scitotenv.2021.149294

Zhang H, Marchant-Forde JN, Zhang X, Wang Y (2020) Effect of cornstalk biochar immobilized bacteria on ammonia reduction in laying hen manure composting. Molecules 27:1560. https://doi.org/10.3390/molecules25071560

Zhang M, Fan D, Su C, Pan L, He Q, Li Z, Liu C (2023) Biotransformation of sulfamethoxazole by a novel strain, *Nitratireductor* sp. GZWM139: characterized performance, metabolic mechanism and application potential. J Hazard Mater 441:0304-3894. https://doi.org/10.1016/j.jhazmat.2022.129861

Zhang Y, Zhao Y, Chen Y, Lu Q, Li M, A XW, Wei Y, Xie X, et al (2016) A regulating method for reducing nitrogen loss based on enriched ammonia-oxidizing bacteria during composting. Bioresour Technol 221:276–283. https://doi.org/10.1016/J.BIORTECH.2016.09.057

Zhao P, Gao X, Liu D, Sun Y, Li M, Han S (2023) Effect of different biochar additions on the change of carbon nitrogen content and bacterial community in meadow soils. Environmental Pollutants and Bioavailability 35:2268272. https://doi.org/10.1080/26395940.2023.2268272

Zhu X, Burger M, Doane TA, Horwath WR (2013) Ammonia oxidation pathways and nitrifier denitrification are significant sources of N_2O and NO under low oxygen availability. Proc Natl Acad Sci U S A 110:6328–6333. https://doi.org/10.1073/pnas.1219993110

Zucconi F (1981) Evaluating toxicity of immature compost. Biocycle 22:54–57